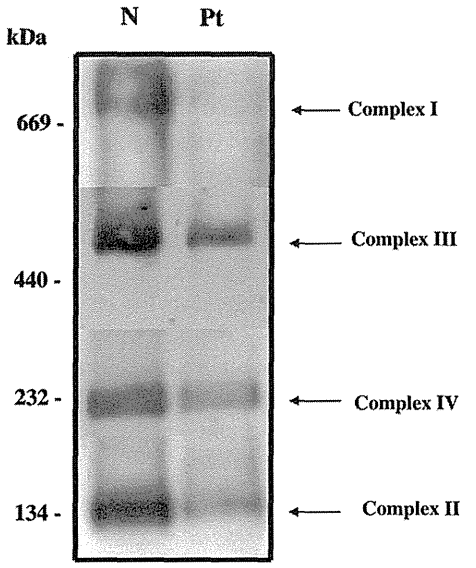

Fig. 2. Blue native polyacrylamide gel electrophoresis (BN-PAGE) analysis of liver respiratory chain enzymes showed markedly decreased protein expression of complex I, while the protein bands of complex II, III, and IV were comparable to the control (N) samples.

Hughes; yet, studies have not progressed because of technical difficulties. More recently, complex I deficiency was regarded as the most common energy generation disorder. The manifestations range from typical mitochondrial diseases, such as Leigh syndrome, to obscure conditions such as slow regression or intractable secretory diarrhea [4].

Complex II activity has been shown to be more labile than complex I when measuring respiratory chain enzymes in patients with a wide range of metabolic disorders, liver failure, or liver disease [5]. In the present case, only complex I activity was very low; this indicates primary complex I deficiency rather than a secondary effect of influenza A infection. Complex I includes seven mitochondrial DNA-encoded subunits and at least 39 nuclear-encoded subunits. In our case, no mutation was detected in the mitochondrial DNA (mtDNA). The detection rate for mutations in mitochondrial or nuclear DNA in complex I deficiency is as small as 20% [6,7].

In the present case, complex I was deficient only in the liver, not in fibroblasts. Mitochondrial respiratory complex disorders can show clinical and biochemical tissue specificity [2,4,6,8,10]. For this reason, it is difficult to diagnose by suspension cells or serum enzyme assays. The possible mechanisms of tissue specificity are tissue-specific subunits of complex I [9], the ratio between normal and mutant mtDNA in a specific tissue [7], and tissue differences in RNA processing [10]. To our knowledge, very few cases with liver-specific complex I deficiency have been reported [2,8]. These reported cases had chronic neurological symptoms such as epilepsy, hypotonia, or developmental regression, with the exception of one case that had severe cardiomyopathy in early infancy [2]. There was one case without evidence of liver dysfunction [8]. Clinically there was no definite difference from usual Co I deficiency. One reason for the small number of cases is that the liver is not the prime diagnostic tissue. Respiratory chain complex deficiency is usually confirmed by tissue biopsy. Muscle is usually the prime diagnostic tissue, and cultured skin fibroblasts are also often analyzed [10]. False-negative diagnostic results may occur because the liver is not examined.

This case was determined to be complex I deficiency by BN-PAGE Western blotting and determination of enzyme activities. This is the first report of respiratory chain complex I deficiency in influenza encephalopathy. We suggest there may be many undiagnosed cases of this metabolic disorder. Here, we described a healthy child, who had never been suspected of having any disease, diagnosed with a metabolic disorder after acute encephalopathy with subsequent death. Future studies are needed to focus on the development of a method to detect this inborn metabolic disorder before onset.

References

[1] Yao D, Mizuguchi H, Yamaguchi M, Yamada H, Chida J, Shikata K, et al. Thermal instability of compound variants of carnitine palmitoyltransferase II and impaired mitochondrial fuel utilization in influenza-associated encephalopathy. Hum Mutat 2008;29:718–27.

[2] Kirby DM, Crawford M, Cleary MA, Dahl HM, Dennett X, Tourburn DR. Respiratory chain complex I deficiency. An underdiagnosed energy generation disorder. Neurology 1999;52:1255–64.

[3] Van Coster R, Smet J, George E, De Meirleir L, Seneca S, Van Hove J, et al. Blue native polyacrylamide gel electrophoresis: a powerful tool of oxidative phosphorylation defects. Pediatr Res 2001;50:658–65.

[4] Murayama K, Nagasaka H, Tsuruoka T, Omata Y, Horie H, Tregoning S, et al. Intractable secretory diarrhea in a Japanese boy with mitochondrial respiratory chain complex I deficiency. Eur J Pediatr 2009;168:297–302.

[5] Hui J, Kirby DM, Thorburn DR, Boneh A. Decreased activities of mitochondrial respiratory chain complexes in non-mitochondrial respiratory chain diseases. Dev Med Child Neurol 2006;48:132–6.

[6] Thorburn DR, Sugiana C, Salemi R, Kirby DM, Worgan L, Ohtake A, et al. Biochemical and molecular diagnosis of mitochondrial respiratory chain disorders. Biochim Biophys Acta 2004;1659:121–8.

[7] Rötig A, Lebon S, Zinovieva E, Mollet J, Sarzi E, Bonnefont JP, et al. Molecular diagnostics of mitochondrial disorders. Biochim Biophys Acta 2004;1659:129–35.

[8] Panetta J, Gibson K, Kirby DM, Thorburn DR, Boneh A. The importance of liver biopsy in the investigation of possible mitochondrial respiratory chain disease. Neuropediatrics 2005;36:256–9.

[9] Clay VJ, Ragan CI. Evidence for the existence of tissue specific isoenzymes of mitochondrial NADH dehydrogenase. Biochem Byophys Res Commun 1988;157:1423–8.

[10] Bindoff LA, Howell N, Poulton J, McCullough DA, Morten KJ, Lightowlers RN, et al. Abnormal RNA processing associated with a novel tRNA mutation in mitochondrial DNA. A potential disease mechanism. J Biol Chem 1993;268:19559–64.

ELSEVIER

Brain & Development 34 (2012) 861–865

BRAIN & DEVELOPMENT
Official Journal of the Japanese Society of Child Neurology

www.elsevier.com/locate/braindev

Case report

Two Japanese patients with Leigh syndrome caused by novel *SURF1* mutations

Junpei Tanigawa [a], Kaori Kaneko [c], Masakazu Honda [d], Hiroko Harashima [d], Kei Murayama [e], Takahito Wada [a], Kyoko Takano [a], Mizue Iai [a], Sumimasa Yamashita [a], Hiroko Shimbo [a], Noriko Aida [b], Akira Ohtake [d], Hitoshi Osaka [a,*]

[a] *Division of Neurology, Kanagawa Children's Medical Center, Yokohama 232-8555, Japan*
[b] *Division of Radiology, Kanagawa Children's Medical Center, Yokohama 232-8555, Japan*
[c] *Division of Pediatric Neurology, Yokohama Ryoiku-iryo Center, Yokohama 241-0014, Japan*
[d] *Department of Pediatrics, Faculty of Medicine, Saitama Medical University, Saitama 350-1241, Japan*
[e] *Department of Metabolism, Chiba Children's Hospital, Chiba 266-0007, Japan*

Received 7 November 2011; received in revised form 11 February 2012; accepted 13 February 2012

Abstract

We report two patients with Leigh syndrome that showed a combination of facial dysmorphism and MRI imaging indicating an *SURF1* deficiency, which was confirmed by sequence analysis. Case 1 is a 3-year-old girl with failure to thrive and developmental delay. She presented with tachypnea at rest and displayed facial dysmorphism including frontal bossing, lateral displacement of inner canthi, esotropia, maxillary hypoplasia, slightly upturned nostril, and hypertrichosis dominant on the forehead and extremities. Case 2 is an 8-year-old boy with respiratory failure. He had been diagnosed as selective complex IV deficiency. Case 2 displayed facial dysmorphism and hypertrichosis. Since both patients displayed characteristic facial dysmorphism and MRI findings, we sequenced the *SURF1* gene and identified two heterozygous mutations; c.49+1 G>T and c.752_753del in Case 1, and homozygous c.743 C>A in Case 2. For patients with Leigh syndrome showing these facial dysmorphism and hypertrichosis, sequence analysis of the *SURF1* gene may be useful.

Keywords: Leigh syndrome; *SURF1* deficiency; Facial dysmorphism; Hypertrichosis

1. Introduction

Leigh syndrome (OMIM 256000) is a progressive neurodegenerative disorder with the usual onset in infancy or early childhood. It is a genetically heterogeneous disease and the most common cause is a molecular defect in mitochondrial energy production system, including the respiratory chain complexes and pyruvate dehydrogenase complex. An isolated generalized defect of complex IV, (Cytochrome C oxidase) is the most common biochemical abnormalities found in Leigh syndrome [1]. Leigh syndrome with *SURF1* mutations, which encode the putative assembly protein of complex IV, have been reported [2] with specific clinical features of facial dysmorphism [3], hypertrichosis [4], and MRI findings [5]. Here, we report two patients with these clinical features and novel *SURF1* mutations.

* Corresponding author. Address: Division of Neurology, Kanagawa Children's Medical Center, 2-138-4 Mutsukawa, Minami-ku, Yokohama 232-8555, Japan. Tel.: +81 45 711 2351; fax: +81 45 721 3324.
E-mail address: hosaka@kcmc.jp (H. Osaka).

0387-7604/$ - see front matter © 2012 The Japanese Society of Child Neurology. Published by Elsevier B.V. All rights reserved.
doi:10.1016/j.braindev.2012.02.007

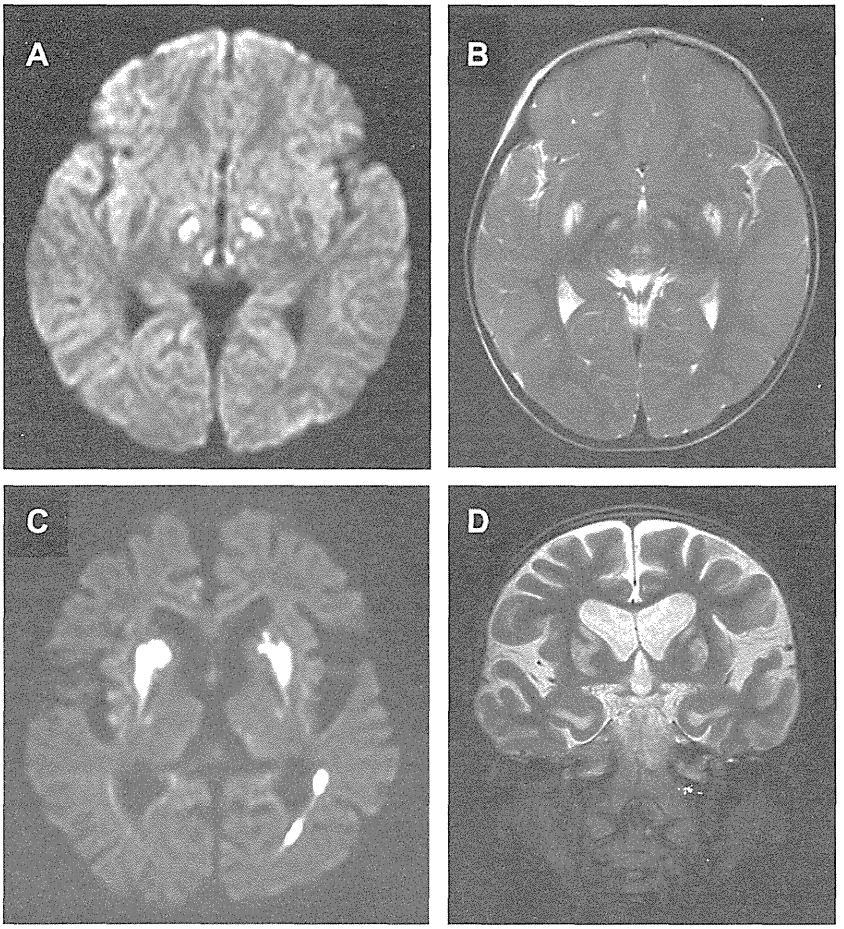

Fig. 1. Diffusion-weighted (A and C) and T2-weighted (B and D) magnetic resonance imaging of the brain in Case 1 at 2 years and 5 months of age (A and B), and in Case 2 at 7 years and 6 months of age (C and D). In Case 1, the bilateral substantia nigra (A), subthalamic nucleus (A and B), red nucleus (A), medial parts of the midbrain (A and B) and putamen (B) show the signal hyperintensity. In Case 2, bilateral striatum reveal hypeintensity (C and D). The left optic radiation is also involved in Case 2 (C) and the global cerebral hemisphere is atrophic (C and D).

2. Case reports

2.1. Case 1

Case 1 is 3-year-old female that was referred to our hospital for an evaluation of failure to thrive and developmental delay at 2 years. She was born to healthy nonconsanguineous Japanese parents. The neonatal period was unremarkable. She held her head upright at 3 months of age, and sat at the 6 months. At the 9 months, she was able to walk independently while holding on to furniture. Her development did not progress thereafter, and she has not walked alone and only speaks using jargon. She was conscious, alert and presented with tachypnea at rest. She displayed facial dysmorphism including frontal bossing, lateral displacement of inner canthi, esotropia, maxillary hypoplasia, slightly upturned nostril, and hypertrichosis dominant on the forehead and extremities. Mild opthalmoplegia and ptosis were noted. She manifested generalized mild hypotonia, truncal ataxia and normal deep tendon reflexes with negative Babinski's signs. Serum lactate was elevated at 35.7 mg/dl. MRI showed signal hyperintensity of the bilateral putamen, subthalamic nucleus, red nucleus and brain stem on T2-weighted images (T2WI) and diffusion-weighted images (DWI) (Fig. 1). The enzyme analysis of the respiratory chain complexes were not performed in this patient.

2.2. Case 2

Case 2 is 8-year-old male on ventilation that was transferred to our hospital for tracheostomy. He was born at term to healthy, nonconsanguineous parents. He had been able to get cruising by 12 months. At 19 months, he presented with neurodevelopmental regression and ataxia. Laboratory investigation revealed elevated cerebrospinal fluid lactate and pyruvate. Brain MRI showed signal hyperintensity of the bilateral basal ganglia, midbrain and medulla oblongata on T2WI. Fibroblast analysis confirmed a decreased amount and activity of complex IV in the respiratory chain complexes

(Fig. 2). He displayed facial dysmorphism including synophrys and micrognathia, hypertrichosis, thoracic deformity and generalized hypotonia and elevated deep tendon reflexes with positive Babinski's signs. MRI showed that the bilateral cerebral hemisphere were globally atrophic and signal hyperintensity of the bilateral optic radiation, putamen, basal ganglia including subthalamic nucleus, and brain stem on T2WI. The left optic radiation, bilateral putamen and globus pallidus also showed high signal intensity on DWI (Fig. 1).

3. Genomic DNA sequencing, RT-PCR and sequencing

Genomic DNA was prepared from white blood cells using the Wizard Genomic DNA purification kit (Promega, Madison, WI, USA). PCR of all exons and exon–intron boundaries of the *SURF1* gene was performed with specific primers using Ex Taq PCR version 1.0 kit (Takara, Shiga, Japan) according to the manufactures instruction (Suppl. Table 1). Total RNA was extracted from leukocytes using Trizol reagent and amplified with the SMART™ mRNA amplification method (Clontech, Mountain View, CA). The amplified mRNA was subjected to reverse transcription with Prime Script reverse transcriptase (Takara, Shiga, Japan) using Oligo (dT) primers. RT-PCR was performed using primers at exons 1 and 9 of the *SURF1* gene, according to the manufacture's instruction (Suppl. Table 1). Patients and families participating in the gene analysis gave written informed consent to the gene analysis, which was approved by the ethical committee of Kanagawa Children's Medical Center.

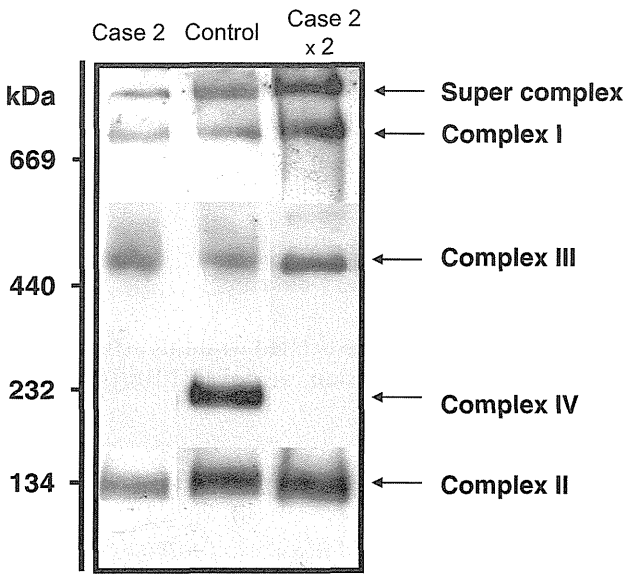

Fig. 2. Analysis of respiratory chain complex amount by blue native polyacrylamide gel electrophoresis in Case 2. Mitochondria isolated from Case 2 and normal control fibroblasts were solubilized in dodecyl maltoside and subjected to BN-PAGE and Western blotting [9]. In x 2 lane, the amount of protein loaded was twice. The amount of fully assembled complex IV was shown to be dramatically decreased in Case 2. The amount of complexes I, II, and III were all comparable to those in the normal control. In vitro enzyme assay [10] also revealed deficiencies of complex IV: the activities of complex I, II, III and IV relative to that of citrate synthase were 137%, 238%, 124% and 12%, respectively.

4. Results

4.1. Case 1

We identified two novel heterozygous mutations: a maternal c.49+1 G>T splice site mutation in intron 1 and a paternal c.752_753del in exon 8. This deletion resulted in a frame shift at amino acid 251(Gln251) causing a stop codon in exon 8 (Fig. 3). The c.49+1 G>T splice site mutation changes the highly conserved G nucleotide at position +1 of the donor splice site (5′ss) in intron 1. We attempted to characterize the splicing outcome of this sequence variation by RT-PCR analysis from patient's blood. Sequence analysis of the RT-PCR reaction detected only the allele with the c.752_753delAG mutation, which implies the presence of a nonsense mediated decay or instability of mRNA from the allele with the c.49+1 G>T splice site mutation.

4.2. Case 2

Sequence analysis of the *SURF1* gene revealed a novel homozygous c.743 C>A, p.Ala248Asp in exon 7. Both parents of this patient were heterozygous for this mutation (Fig. 3). This mutation changes highly conserved Alanine to Aspartate. This mutation was not found in 100 control alleles.

5. Discussion

Molecular elucidation of Leigh syndrome is challenging since many enzymes are involved, such as mitochondrial respiratory chain complexes I, II, III, IV, and V, and components of the pyruvate dehydrogenase complex. Mutation analysis in DNA is more complicated, even after focusing on respiratory complex IV. Mitochondrial-encoded *MTCO3* and nuclear-encoded *COX10*, *COX15*, *SCO2*, and *SURF1*, have been reported as the cause of Leigh syndrome [6,7]. Our two cases presented with mental retardation, failure to thrive, respiratory dysfunction, facial dysmorphism and hypertrichosis. Facial dysmorphism including micrognathia and hypertrichosis especially in the extremities have been reported to be distinctive and characteristic feature of *SURF1* gene mutation [3,4]. Our two cases underscore the importance of *SURF1* analysis in Leigh syndrome with facial dysmorphism and hypertrichosis. However, not all patients with this gene mutation carry these symptoms. Although facial dysmorphism has been also

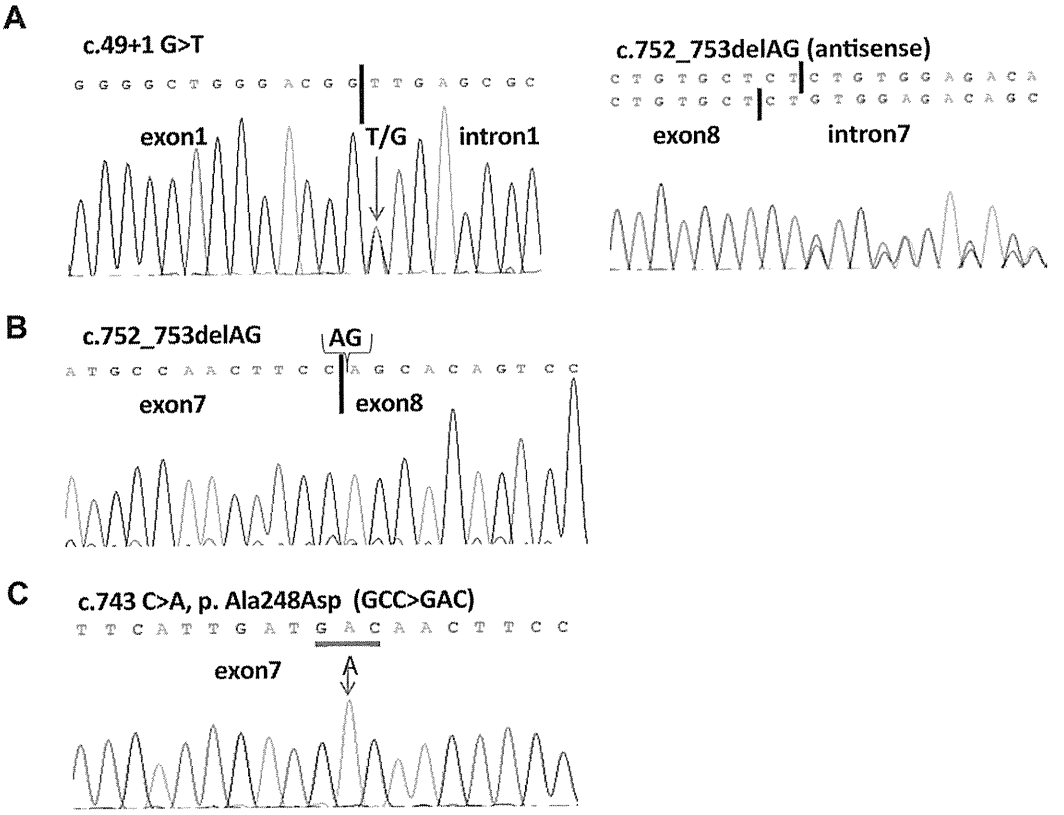

Fig. 3. Analysis of the *SURF1* gene. A chromatogram of the two novel heterozygous mutations; c.49+1 G>T and c.752_753del in Case 1 (A) and homozygous c.743 C>A in Case 2 (C). Panel B shows the chromatogram of cDNA from Case 1. The mutations are shown on the sense strand except for the right panel of A (antisense).

reported in Leigh syndrome with pyruvate dehydrogenase complex, hypertrichosis has not been described [8].

To date, more than 100 patients of Leigh disease with *SURF1* mutations have been reported [6,7]. To our knowledge, this is the first report of a mutation in intron 1, suggesting the need to scan whole exons and exon/intron boundaries.

Common MRI findings of Leigh syndrome are symmetric lesions in the brainstem, basal ganglia, thalamus and spinal cord, Leigh syndrome with *SURF1* mutation have been reported to involved the subthalamic nuclei, medulla, inferior cerebellar peduncles, and substantia nigra [5]. In addition, Case 2 showed signal hyperintensities in bilateral optic radiation on T2WI and DWI, which has not been reported previously in Leigh syndrome with *SURF1* mutations. Since Case 2 had never shown severe hypoxemia, this finding may be significant in patients with *SURF1* mutation or may appear in a progressed stage of disease.

Acknowledgements

This work was supported in part by Grants-in-Aid from Scientific Research from the Ministry of Health, Labor and Welfare of Japan, Health and Labor Science Research Grant of Japan, Yokohama Foundation for Advancement of Medical Science, Takeda Science Foundation, Kanagawa Municipal Hospital Pediatric Research and a grant of the Innovative Cell Biology by Innovative Technology (Cell Innovation Program) from the Ministry of Education, Culture, Sports, Science and Technology, Japan.

Appendix A. Supplementary data

Supplementary data associated with this article can be found, in the online version, at doi:10.1016/j.braindev.2012.02.007.

References

[1] Rahman S, Blok RB, Dahl HH, Danks DM, Kirby DM, Chow CW, et al. Leigh syndrome: clinical features and biochemical and DNA abnormalities. Ann Neurol 1996;39:343–51.
[2] Zhu Z, Yao J, Johns T, Fu K, De Bie I, Macmillan C, et al. SURF1, encoding a factor involved in the biogenesis of cytochrome c oxidase, is mutated in Leigh syndrome. Nat Genet 1998;20:337–43.
[3] Yüksel A, Seven M, Cetincelik U, Yeşil G, Köksal V. Facial dysmorphism in Leigh syndrome with SURF-1 mutation and COX deficiency. Pediatr Neurol 2006;34:486–9.
[4] Ostergaard E, Bradinova I, Ravn SH, Hansen FJ, Simeonov E, Christensen E, et al. Hypertrichosis in patients with SURF1 mutations. Am J Med Genet A 2005;138:384–8.

[5] Rossi A, Biancheri R, Bruno C, Di Rocco M, Calvi A, Pessagno A, et al. Leigh Syndrome with COX deficiency and SURF1 gene mutations: MR imaging findings. AJNR Am J Neuroradiol 2003;24:1188–91.
[6] Shoubridge EA. Cytochrome c oxidase deficiency. Am J Med Genet 2001;106:46–52.
[7] Böhm M, Pronicka E, Karczmarewicz E, Pronicki M, Piekutowska-Abramczuk D, Sykut-Cegielska J, et al. Retrospective, multicentric study of 180 children with cytochrome C oxidase deficiency. Pediatr Res 2006;59:21–6.
[8] Robinson BH, MacMillan H, Petrova-Benedict R, Sherwood WG. Variable clinical presentation in patients with defective E1 component of pyruvate dehydrogenase complex. J Pediatr 1987;111:525–33.
[9] Kirby DM, Salemi R, Sugiana C, Ohtake A, Parry L, Bell KM, et al. NDUFS6 mutations are a novel cause of lethal neonatal mitochondrial complex I deficiency. J Clin Invest 2004;114:v837–845.
[10] Murayama K, Nagasaka H, Tsuruoka T, Omata Y, Horie H, Tregoning S, et al. Intractable secretory diarrhea in a Japanese boy with mitochondrial respiratory chain complex I deficiency. Eur J Pediatr 2009;168:297–302.

PEDIATRICS INTERNATIONAL Official Journal of the Japan Pediatric Society

Pediatrics International (2013) **55**, e103–e106 doi: 10.1111/ped.12098

Patient Report

Case of an infant with hepatic cirrhosis caused by mitochondrial respiratory chain disorder

Shigehiro Enkai,[1] Sachi Koinuma,[2] Reiko Ito,[2] Junko Igaki,[3] Yukihiro Hasegawa,[3] Kei Murayama[4] and Akira Ohtake[5]

[1]*Department of Pediatrics, Fussa Hospital,* [2]*Division of Gastroenterology, National Center for Child Health and Development,* [3]*Division of Endocrinology and Metabolism, Tokyo Metropolitan Children's Medical Center, Tokyo,* [4]*Division of Metabolism, Chiba Children's Hospital, Chiba, and* [5]*Department of Pediatrics, Faculty of Medicine, Saitama Medical University, Saitama, Japan*

Abstract The patient had hepatomegaly with liver dysfunction at the age of 1 month. Magnetic resonance imaging performed at the age of 1 year showed multiple nodules of varying size in his liver. We were able to examine the mitochondrial respiratory chain function in the liver biopsy samples because all other differential diagnoses for hepatic cirrhosis had been ruled out. Complex I and IV activities were below the normal level (<30%) of the citrate synthase (CS) ratio. Liver blue native polyacrylamide gel electrophoresis showed an extremely weak complex I and IV band. Liver respiratory chain complexes I and IV were found to be deficient in this patient. The histologic findings were highly suggestive of mitochondrial respiratory chain disorder. Findings of progressive liver cirrhosis changes were observed in magnetic resonance imaging at the age of 5 years. An examination of the mitochondrial respiratory chain function should be performed along with a liver biopsy if mitochondrial respiratory chain disorder is suspected as a possible differential diagnosis of idiopathic hepatitis.

Key words chronic hepatitis, infant, liver cirrhosis, mitochondrial respiratory chain complex I and IV deficiency, mitochondrial respiratory chain disorder.

Mitochondrial respiratory chain disorder (MRCD), which is caused by the loss of one or more enzyme activities in respiratory chain complexes I–IV, has many clinical manifestations in various organs and is a known cause of mitochondrial encephalomyopathy, idiopathic hepatitis and idiopathic muscle weakness. Although MRCD is one of the differential diagnoses for hepatic disorder, it is not actively diagnosed. The early diagnosis of MRCD in the liver is important because some patients will subsequently develop liver cirrhosis or liver failure.[1,2] This report is based on a boy with chronic hepatic disorder and cirrhosis who was found to have mitochondrial respiratory chain complex I and IV deficiencies during his infant period.

Case Report

The patient was a Japanese boy born at term and weighing 3296 g; he was the second child of healthy parents with consanguinity. His elder sister (3 years old) is presently in good health. The mother's brother (31 years old) was found to have hepatic dysfunction during his infant period and his condition progressed to cirrhosis during adulthood. The proband's weight gain after birth was good. Jaundice and hepatomegaly were observed at the age of 1 month and he was admitted to our hospital. Upon admission (32 days after birth), he exhibited conjunctival icterus, his liver was palpable 5 cm below the right costal margin, he had normal muscle tone and no external malformations were noted. His laboratory data on admission showed cholestatic hepatitis. Tandem mass spectrometry, urine organic acid and bile acid analysis were normal. The following differential diagnoses were ruled out: autoimmune disease, infectious disease, disorder of organic acid metabolism and fatty acid oxidation, alpha 1-antitrypsin deficiency, tyrosinemia, galactosemia, and citrin deficiency. Furthermore, respiratory disorder, abnormal findings on skin or bone, and susceptibility to infection, which are the main symptoms of Langerhans cell histiocytosis and cystic fibrosis, are not present in this patient at the current age of 6 years. Imaging studies did not reveal any congenital portal venous or portal biliary tract malformations. The patient's transaminase (aspartate aminotransferase [AST] and alanine aminotransferase [ALT]) levels were 78–477 IU/l (AST) and 13–181 IU/l (ALT) and fluctuated with his physical condition. The patient's γ-GTP levels decreased to a normal range before the age of 6 months. Throughout the clinical course, the patient's blood lactate and pyruvic acid levels were almost always normal. Hypoglycemia was not observed during follow-up examinations. He exhibited normal growth and development. An abdominal magnetic resonance imaging (MRI) examination performed at the age of 2 months was normal except for hepatomegaly. However, an abdominal MRI performed at 1 year and 4 months showed multiple nodules of varying size in his liver, which appeared

Correspondence: Shigehiro Enkai, MD, Department of Pediatrics, Fussa Hospital, 1-6-1 Kamidaira, Fussa, Tokyo 197-0012, Japan. Email: enkai@fussahp.jp

Received 5 January 2012; revised 17 January 2013; accepted 19 February 2013.

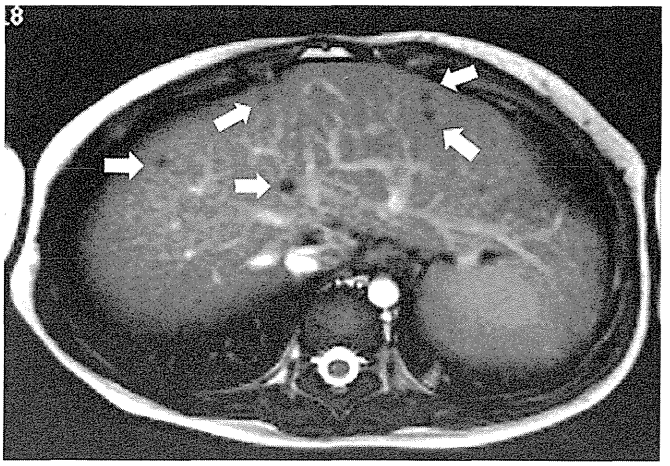

Fig. 1 Abdominal magnetic resonance image obtained at 1 year and 4 months shows multiple nodules (arrows) varying in size in the liver, which presented as a low-intensity area on T2-weighted imaging.

as low-intensity areas on T2-weighted images (see Fig. 1) and high-intensity areas on T1-weighted images without contrast enhancement. The number of nodules in his liver increased from the time of the MRI examination performed at the age of 1 year and 4 months. In addition, a transient elevation in the patient's serum ammonia levels (290 μg/dL) and impaired consciousness with the onset of fever and a poor appetite were observed at the age of 2 years. The clinical course during this episode showed positive results. Liver biopsies were performed during a laparotomy to inspect the progress of the liver cirrhosis at the age of 2 years and 1 month. He was suspected of having MRCD, which is one of the main causes of hepatic disorder, because all other differential diagnoses for hepatic cirrhosis had been ruled out. Thus, we were able to examine the mitochondrial respiratory chain function in the liver biopsy samples. Liver respiratory chain complexes I and IV were found to be deficient in this patient using both a respiratory chain enzyme assay (Table 1) and a liver blue native polyacrylamide gel electrophoresis (BN-PAGE).[3] Complex I and IV activities were below the normal level (<30%)[4] of the CS ratio. Liver BN-PAGE showed an extremely weak complex I and IV band in this patient. In addition, the rate of mtDNA and nDNA (quantitative polymerase chain reaction) was about 95.4% (normal level). Mitochondrial DNA depletion syndrome was ruled out. The macroscopic anatomy showed diffuse nodules on the surface of the liver. The microscopic findings for the liver are shown in Figure 2. Coenzyme Q, vitamin C, vitamin E, and carnitine therapy were initiated at an age of 2 years and 3 months. The patient continues to exhibit normal physical and mental development after diagnosis. His weight was 21.9 kg (+0.3SD score) and height was 117.5 cm (+0.6SD score) at the age of 6 years. However, the patient's transaminase levels were 56–311 IU/L (AST) and 31–174 IU/L (ALT), and findings of the follow-up MRI at the age of 5 years suggested progressive changes in liver cirrhosis. MRI demonstrated right lobe atrophy, enlargement of the left lobe, and an irregular edge border of the liver (Fig. 3a,b). MRI revealed a well-circumscribed mass 16 × 11-mm (see arrow) in liver segment VI (Fig. 3c). In addition to this mass, MRI demonstrated nodules 4–8 mm in size in the liver parenchyma, which were visualized as slightly hyperintense lesions on the T2-weighted images and as hypointensities on the T1-weighted images (Fig. 3c).

Table 1 Respiratory chain enzyme assay in the liver of the patient

	Complex I	Complex II	Complex III	Complex IV	CS
% of normal	14	37	62	15	54
CS ratio (%)	26	67	111	27	
Complex II ratio (%)	38		165	40	

Discussion

We reported a boy with chronic hepatic disorder and cirrhosis who was found to have mitochondrial respiratory chain complex I and IV deficiency during his infant period. In our experience, deficiencies of complexes I and IV account for about 15% of all diagnosed cases of MRCD in Japanese subjects. Nine clinical case reports of complex I and IV deficiencies, including adult subjects, were reported between 1988 and 2010. No specific manifestations of complex I and IV deficiency were observed in the past reports. The patient's blood lactate/pyruvate rate was almost normal in the clinical course. However, a normal lactate level does not exclude respiratory chain defects in MRCD, including mitochondrial hepatopathy.[5,6] The molecular and genetic causes of complex I and IV deficiency are not clear.

The histological findings of liver biopsy specimens from patients with primary mitochondrial hepatopathies reveal individual, non-specific histologic and ultrastructural findings, with predominant microvesicular steatosis and canalicular cholestasis.[7] Periportal and centrilobular fibrosis are characteristic features, and the dropout of broad bands of hepatocytes leads to micronodular cirrhosis.[7] Thus, the histologic findings of this case were highly suggestive of MRCD. In addition, if electron micrographs revealed morphological abnormality of mitochondria in liver biopsies, they would have been useful for confirming diagnosis of MRCD.

With respect to MRI findings, nodules which were found at the age of 1 year were not detected at the age of 5 years. The nodules in Figure 1 might be regenerative nodules (RN) associated with hepatic cirrhosis, because RN typically appear as hypointense lesions on T2-weighted images[8] and the imaging findings at the age of 5 years were typical of hepatic cirrhosis. Furthermore, focal nodular hyperplasia, which is one of the important differential diagnoses of hepatic nodules in infants, was excluded on the basis of the high signal intensity in the non-enhanced T2-weighted images.[9] However, these nodules were so small that they were difficult to evaluate by MRI or histopathology.

Findings of progressive liver cirrhosis changes were observed in a liver MRI at the age of 5 years (Fig. 3a–c). The 16 × 11-mm mass in Figure 3c (see arrow) was visualized as a hyperintensity on opposed-phase T1-weighted gradient-echo images and as a slightly low-intensity area on the T2-weighted images. Focal

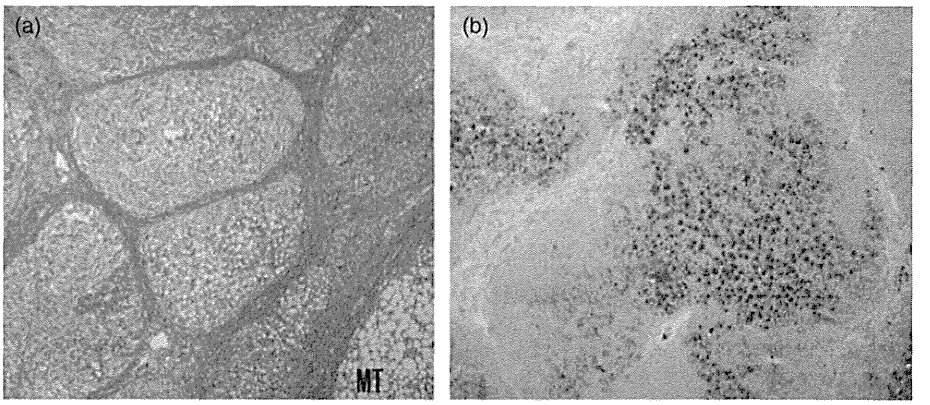

Fig. 2 (a) Masson trichrome stain: Microscopic findings in the liver show the division of a hepatic lobule into nodules by bridging fibrosis in the liver tissue. (b) Sudan III stain: Liver tissues show heterogeneous hepatic steatosis in each septum. Portal fibrosis was observed in liver tissues without inflammation (not shown).

nodular hyperplasia was excluded because the mass did not show the high-intensity on the non-enhanced T2-weighted images. The size remained unchanged as compared to the previous year. Thus, the mass was suspected to be a regenerative nodule or adenomatous hyperplasia, associated with hepatic cirrhosis. In addition to this mass, MRI in Figure 3c demonstrated nodules 4–8 mm in size in the liver parenchyma. Although these nodules were found to contain lipids inside, as they were visualized as low-intensity areas on opposed-phase T1-weighted gradient-echo images and as high-intensity areas on in-phase images, they were too small to evaluate in detail.

The early and accurate diagnosis of MRCD is important because appropriate therapy and guidance can be provided to the patient and his/her family before the condition worsens. MRCD is difficult to diagnose because the clinical manifestations do not depend on the type of complex deficiency. Some previous patients have died of hepatic failure during the neonatal period or infancy, while other patients never develop hepatic disease despite long-term follow-up observation.[1] However, it is conceivable that a regular screening for secondary liver cancer is necessary for the patient with progressive cirrhosis, along with MRCD during his infant period.[10]

With respect to diagnosis, regular ultrasound or CT examinations are needed for infants with idiopathic chronic hepatitis because multiple nodules in the liver gradually appeared in the patient. Furthermore, we conclude that an examination of the mitochondrial respiratory chain function should be performed along with a liver biopsy if MRCD is suspected as a possible differential diagnosis of idiopathic hepatitis under the signs of liver cirrhosis, as in this case.

Acknowledgments

The authors report no conflicts of interest. We have no disclosures to make and have not received any financial support.

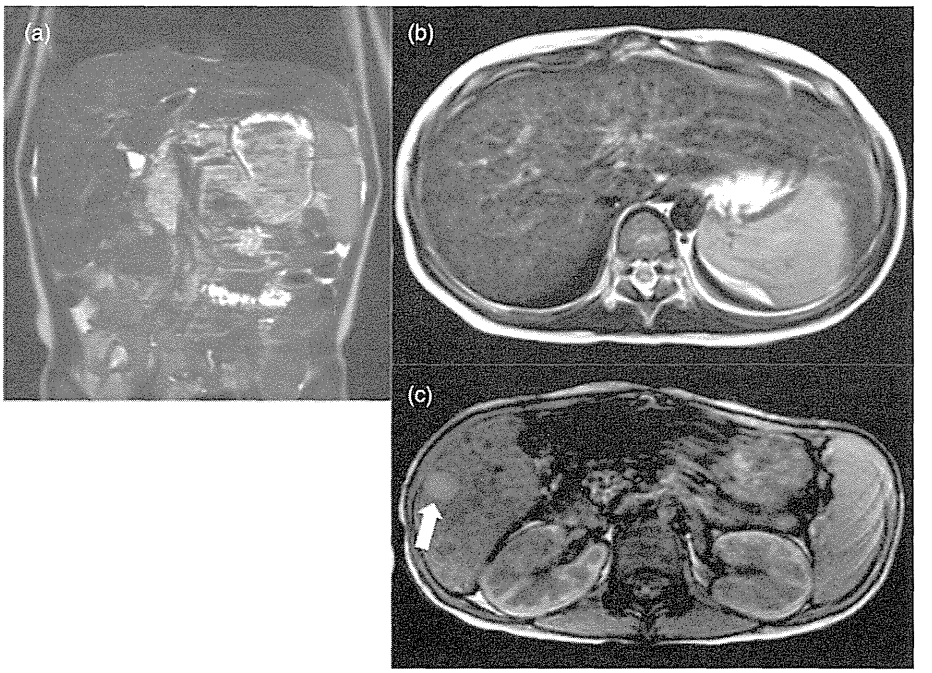

Fig. 3 (a) T2-weighted magnetic resonance image (MRI) demonstrates right lobe atrophy, enlargement of the left lobe, and an irregular edge border of the liver at the age of 5 years. (b) T2-weighted MRI shows marked hyperintensity in the periportal region. The hepatic parenchyma appears heterogeneously enhanced in the delayed phase. (c) T1-weighted MRI revealing a well-circumscribed 16 × 11-mm mass (see arrow) in liver segment VI. This mass is visualized as a hyperintensity on opposed-phase T1-weighted gradient-echo images and as a slightly lower-intensity area on the T2-weighted images. In addition to this mass, MRI demonstrates nodules 4–8 mm in size in the liver parenchyma, which are visualized as slightly hyperintense lesions on the T2-weighted images and as hypointensities on the T1-weighted images.

References

1 Carcia-cazorla A, De Lonlay P, Rustin P *et al.* Mitochondrial respiratory chain deficiencies expressing the enzymatic deficiency in the hepatic tissue: a study of 31 patients. *J. Pediatr.* 2006; **149**: 401–5.
2 Lee WS, Sokol RJ. Mitochondrial hepatopathies: advances in genetics and pathogenesis. *Hepatology* 2007; **45**: 1555–65.
3 Schagger H, Aquila H, von Jagow G. Coomassie blue-sodium dodecyl sulfate- polyacrylamide gel electrophoresis for direct visualization of polypeptides during electrophoresis. *Anal. Biochem.* 1988; **173**: 201–55.
4 Bernier FP, Boneh A, Dennett X, Chow CW, Cleary MA, Thorburn DR. Diagnostic criteria for respiratory chain disorders in adults and children. *Neurology* 2002; **59**: 1406–11.
5 Kirby MD, Crawford M, Cleary MA, Dahl HH, Dennet X, Thorburn DR. Respiratory chain complex I deficiency: an underdiagnosed energy generation disorder. *Neurology* 1999; **52**: 1255–64.
6 Fellman V, Kotarsky H. Mitochondrial hepatopathies in the newborn period. *Semin. Fetal Neonatal Med.* 2011; **16**: 222–8.
7 Suchy FJ, Sokol RJ, Balistreri WF. *Liver Disease in Children*, 3rd edn. Cambridge University Press, Cambridge, 2007; 803–29.
8 Hussain SM, Terkivatan T, Zondervan PE *et al.* Focal nodular hyperplasia: Findings at state-of-the-art MR imaging, US, CT, and pathologic analysis. *Radiographics* 2004; **24**: 3–17.
9 Hanna RF, Aguirre DA, Kased N, Emery SC, Peterson MR, Sirlin CB. Cirrhosis-associated hepatocellular nodules: correlation of histopathologic and MR imaging features. *Radiographics* 2008; **28**: 747–69.
10 Scheers I, Bachy V, Stephenne X, Sokal EM. Risk of hepatocellular carcinoma in liver mitochondrial respiratory chain disorders. *J. Pediatr.* 2005; **146**: 414–7.

Mitochondrion 13 (2013) 881–887

Contents lists available at ScienceDirect

Mitochondrion

journal homepage: www.elsevier.com/locate/mito

Polymorphic mutations in mouse mitochondrial DNA regulate a tumor phenotype

Gaku Takibuchi [a], Hirotake Imanishi [a,b,c], Mami Morimoto [a], Kaori Ishikawa [a], Kazuto Nakada [a,d], Noriko Toyama-Sorimachi [c], Yoshiaki Kikkawa [e], Keizo Takenaga [f], Jun-Ichi Hayashi [a,d,*]

[a] Faculty of Life and Environmental Sciences, University of Tsukuba, 1-1-1 Tennodai, Tsukuba, Ibaraki 305-8572, Japan
[b] Japan Society for the Promotion of Science (JSPS), 8 Ichiban-cho, Chiyoda-ku, Tokyo 102-8472, Japan
[c] Department of Molecular Immunology and Inflammation, Research Institute, National Center for Global Health and Medicine, 1-21-1 Toyama, Shinjuku-ku, Tokyo 162-8655, Japan
[d] International Institute for Integrative Sleep Medicine (WPI-IIIS), University of Tsukuba, 1-1-1 Tennodai, Tsukuba, Ibaraki 305-8572, Japan
[e] Mammalian Genetics Project, Tokyo Metropolitan Institute of Medical Science, 2-1-6 Kami-kitazawa, Setagaya-ku, Tokyo 156-8506, Japan
[f] Department of Life Science, Shimane University Faculty of Medicine, 89-1 Enya-cho, Izumo, Shimane 693-8501, Japan

ARTICLE INFO

Article history:
Received 11 March 2013
Received in revised form 17 July 2013
Accepted 30 July 2013
Available online 6 August 2013

Keywords:
Transmitochondrial cybrids
Mouse C3H mtDNA
Polymorphic mtDNA mutations
Tumor phenotypes
Hypoxia sensitivity

ABSTRACT

To examine whether polymorphic mtDNA mutations that do not induce significant respiration defects regulate phenotypes of tumor cells, we used mouse transmitochondrial tumor cells (cybrids) with nuclear DNA from C57BL/6 (B6) strain and mtDNA from allogenic C3H strain. The results showed that polymorphic mutations of C3H mtDNA in the cybrids induced hypoxia sensitivity, resulting in a delay of tumor formation on their subcutaneous inoculation into B6 mice. Therefore, the effects of polymorphic mutations in normal mtDNA have to be carefully considered, particularly when we apply the gene therapy to the embryos to replace their pathogenic mtDNA by normal mtDNA.

1. Introduction

Accumulation of the mtDNA with pathogenic mutations that induce significant mitochondrial respiration defects can be responsible for mitochondrial diseases (Taylor and Turnbull, 2005; Wallace, 2005), and is involved in aging and age-associated disorders (Jacobs, 2003; Khrapko and Vija, 2008; Loeb et al., 2005; Taylor and Turnbull, 2005; Wallace, 2005). Moreover, accumulation of somatic mutations in mtDNA with age can also be involved in tumor development, since some of the somatic mtDNA mutations induce mitochondrial respiration defects, resulting in upregulation of aerobic glycolysis (the Warburg effect) (Taylor and Turnbull, 2005; Wallace, 2005). Our previous studies showed that specific mtDNA mutations regulate tumor phenotypes as a consequence of overproduction of the reactive oxygen species (ROS) and the resultant induction of genetic instability (Hashizume et al., 2012; Imanishi et al., 2011; Ishikawa et al., 2008).

As animal models for these mtDNA-based disorders, our previous studies generated transmitochondrial mito-miceΔ carrying mtDNA with a pathogenic deletion mutation (ΔmtDNA) (Inoue et al., 2000; Nakada et al., 2001), and succeeded in generation of their healthy progeny via nuclear transplantation from one-cell embryos into enucleated oocytes with normal mtDNA (Sato et al., 2005). Subsequently, the nuclear transplantation was applied in primate (Tachibana et al., 2009) and human embryos (Craven et al., 2010; Paull et al., 2013; Tachibana et al., 2013). However, one of the most important problems that have to be solved before applying the nuclear transplantation technology to human cases is the influence of polymorphic mutations in normal mtDNA from the oocyte donors on the phenotypes of the progeny, even when the polymorphic mtDNA mutations do not induce significant respiration defects. In fact, some polymorphic mutations in mouse mtDNA were proposed to affect on age-related hearing loss (Johnson et al., 2001), learning retardation (Roubertoux et al., 2003), delay of cell proliferation (Moreno-Loshuertos et al., 2006), and defects in behavior (Sharpley et al., 2012).

Our previous study (Ishikawa et al., 2010) revealed a novel role of polymorphic mutations in mtDNA: innate immune system in C57BL/6 (B6) strain mice can recognize polymorphic mutations in mtDNA from allogenic NZB strain mice, resulting in suppression of tumor formation of transmitochondrial tumor cells with NZB mtDNA (P29mtNZB cybrids) in B6 mice. The P29mtNZB cybrids possessed syngenic B6 strain-derived nuclear DNA from P29 tumor cells but possessed mtDNA from allogenic NZB strain mice. On the contrary, P29mtC3H cybrids with allogenic C3H mtDNA were able to form tumors, but

* Corresponding author at: Graduate School of Life and Environmental Sciences, Institute of Biological Sciences, University of Tsukuba, 1-1-1 Tennodai, Tsukuba, Ibaraki 305-8572, Japan. Tel./fax: +81 298536650.
E-mail address: jih45@biol.tsukuba.ac.jp (J.-I. Hayashi).

1567-7249/$ – see front matter
http://dx.doi.org/10.1016/j.mito.2013.07.117

showed latency periods to form detectable tumor masses longer than those of P29mtB6 cybrids with syngenic B6 mtDNA.

This study addressed the issue of how polymorphic mutations in mtDNA from allogenic C3H strain induce the delay of tumor formation of P29mtC3H cybrids under the skin of B6 mice.

2. Materials and methods

2.1. Cell lines and cell culture

Transmitochondrial tumor cybrids P29mtB6 and P29mtC3H, which were obtained in our previous report (Ishikawa et al., 2010), were grown in normal medium [DMEM + pyruvate (0.1 mg/ml) + uridine (50 mg/ml) + 10% FBS] in either normoxia (21% O_2) or hypoxia (7% O_2). For treatment with N-acetylcysteine (NAC) (Sigma), cybrids were grown in normal medium supplemented with 20 mM NAC for 48 h.

2.2. Mouse strains

Mice of the inbred strain B6 were obtained from CLEA Japan, Inc. The B6mtC3H mice were generated in our previous study (Kasahara et al., 2006). They showed normal lifespan and no detectable abnormalities (Hashizume et al., 2012). The immunodeficient B6 $Rag2^{-/-}/\gamma c^{-/-}$ mice were provided by S. Koyasu and S. Nagai (Keio University School of Medicine, Shinju-ku, Tokyo, Japan). These mice share B6 nuclear DNA background. The mice were cared for in accordance with the Guide for the Care and Use of Laboratory Animals. Experiments using these mice were approved by the Animal Care and Use Committee of University of Tsukuba and the Research Institute National Center for Global Health and Medicine.

2.3. Assay of tumor formation and metastasis

For testing tumor formation phenotypes, 5×10^6 cells or 5×10^3 cells in 100 μl PBS were inoculated subcutaneously into the back of 5-week-old male B6 mice. Maximum (a) and minimum (b) diameters and height (h) of tumors were recorded twice per week. The volume of each tumor (V) was calculated according to the formula: $V = \pi abh/6$. To examine spontaneous metastasis, 5×10^6 cells in 100 μl PBS were injected s.c. into the back of 5-week-old male B6 mice. The recipient mice were sacrificed when the tumor volume reached 500 mm^3, and their lungs were removed, and then parietal nodules were counted.

2.4. Estimation of doubling times

Growth capacity was determined by plating 1×10^4 cells on 6-well plates in 2 ml of the normal medium, incubated at 37 °C for 5 days, and performing cell counts at daily intervals.

2.5. Cell invasion assay

The invasive ability of the cells was assayed using cell culture inserts (8 μm pore size) for 24-well plates coated with Matrigel, according to the manufacturer's instructions (Becton, Dickinson). Total numbers of 2.5×10^4 cells were seeded and incubated for 24 h at 37 °C. Then, the number of invaded cells on the lower surface of the membrane was counted under a light microscope. Each experiment was performed in triplicate.

2.6. Cell migration assay

The ability of cell migration was detected using non-coated cell culture inserts (8 μm pore size) for 24-well plates according to the manufacturer's instructions (Becton, Dickinson). For testing cell migration, 1.25×10^4 cells were seeded, and after incubation for 24 h at 37 °C, the number of migrated cells on the lower surface of the membrane was counted under a light microscope. Each experiment was performed in triplicate.

2.7. Histological analysis

Cytochemical analysis for cytochrome *c* oxidase (COX) activity was carried out based on the procedures as described previously (Seligman et al., 1968) with slight modifications (Mito et al., 2013).

2.8. Measurement of mitochondrial ROS

Mitochondrial ROS generation was estimated using MitoSOX-Red mitochondrial superoxide indicator (Invitrogen) and Amplex Red Hydrogen Peroxide/Peroxidase Assay kit (Invitrogen). In mitochondrial superoxide measurement, cells were incubated with 5 μM MitoSOX-Red for 20 min at 37 °C in serum-free DMEM, washed twice with serum-free DMEM, and then immediately analyzed with a FACSCalibur Flow Cytometer (Becton Dickinson). The hydrogen peroxide (H_2O_2) levels in isolated mitochondria from the cybrids were measured using the HRP-linked fluorometric assay. Isolated mitochondria (10–20 μg in 50 μl volume) were added to 96 well plate in triplicate with a total reaction volume of 100 μl of reaction buffer containing 0.1 U/ml HRP, and 50 μM Amplex Red reagents. Fluorescence was measured using a SpectraMax 190 Absorbance Microplate Reader (Molecular Devices) at room temperature. The H_2O_2 concentrations were calculated from standard curve and normalized with per mg protein.

2.9. Measurement of lactate

Cells were seeded at 5×10^4 cells/well of a 12-well plate and cultured for 24 h. The amounts of lactates in the cell medium were estimated using an F-kit L-Lactic acid (Roche, Basel, Switzerland).

2.10. SDS-PAGE and Western blotting

Cells were lysed in 1% Nonidet P-40, 150 mM NaCl, 10% glycerol, 2 mM EDTA, 20 mM Tris–HCl (pH 8.0), 1 mM dithiothreitol, 1 mM phenylmethylsulfonyl fluoride (PMSF), protease inhibitor mixture (Roche Diagnostics GmbH, Mannheim, Germany) and phosphatase inhibitor cocktail (PhosSTOP, Roche) for 20 min on ice. After centrifugation at 10,000 *g* for 10 min at 4 °C, the supernatants were used for further analyses. Protein concentration in the supernatants was determined by the method of Bradford using bovine serum albumin (BSA) as a standard. Proteins were resolved by SDS-PAGE under reducing conditions and the resolved proteins were transferred electrophoretically to Immobilon-P Transfer Membrane (Merck Millipore, Japan). After incubating with 10% BSA in TBS–T (150 mM NaCl, 50 mM Tris–HCl (pH 7.4), 0.05% Tween 20) for at least 1 h at room temperature, the membrane was incubated with polyclonal antibody for the appropriate time, washed extensively with TBS–T, and then incubated with horseradish peroxidase-conjugated goat anti-rabbit IgG. Anti-p-IkBα (S32), anti-IkB, anti-pAKT (S473), anti-AKT, anti-pAMPKα (T172), anti-AMPKα and anti-LC3B were obtained from Cell Signaling Technology (Japan), and anti-BCL-2, anti-BCL-X_L, anti-MCL-1, anti-BAX, and anti-β-actin were from Santa Cruz Biotechnology Inc. (Santa Cruz, CA). Anti-α-tubulin was obtained from Sigma-Aldrich. Monoclonal anti-HIF-1α antibody was obtained from Novus Biologicals, Littleton, CO, USA. Proteins were detected using Amersham ECL Western blotting detection reagents (GE Healthcare, Buckinghamshire, UK).

2.11. Assay of hypoxia viability

Hypoxia viability was determined by plating 1×10^5 cells on 6-well plates in 2 ml of medium and cultured at 37 °C for 5 days in hypoxic conditions (<0.1% O_2) using an Anaero Pack (SGI, A-07). After

incubation, live cells (l) and dead cells (d) were counted using trypan blue. Hypoxia viability (hv) was estimated according to the formula: $hv = l/(l + d)$.

2.12. Statistical analysis

The data were analyzed with a Student's *t* test. All values are the mean ± S.D., and *P* values < 0.05 were considered to be statistically significant.

3. Results

3.1. Identification of candidate mtDNA mutations inducing a delay of tumor formation

First, we confirmed a delay of tumor formation of P29mtC3H cybrids in B6 mice using P29mtB6 and P29mtC3H cybrids obtained in our previous study (Ishikawa et al., 2010). The longer latency periods of P29mtC3H cybrids than those of P29mtB6 cybrids were emphasized on inoculation of lower numbers of the cybrids into B6 mice (Fig. 1A). Moreover, the latent periods observed on inoculation of 5×10^6 P29mtC3H cybrids corresponded to those observed on inoculation of 5×10^3 P29mtB6 cybrids, suggesting the significant suppression of tumor formation of P29mtC3H cybrids in B6 mice. On the contrary, no substantial differences between P29mtB6 and P29mtC3H cybrids were observed in tumor growth curves (Fig. 1A). Moreover, both cybrids formed no metastatic nodules in the lungs on their inoculation under the skin of B6 mice. They also showed similar tumor-related phenotypes, such as, doubling times (Fig. 1B), invasion (Fig. 1C), and migration (Fig. 1D) under the culture conditions.

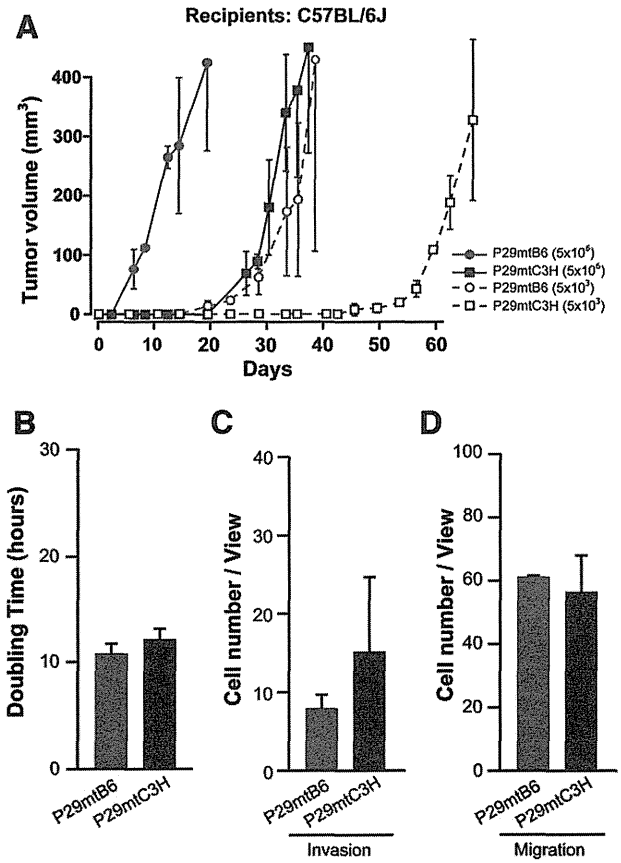

Fig. 1. Comparison of tumor-related phenotypes between P29mtB6 and P29mtC3H cybrids. (A) Tumor formation of the cybrids. Total numbers of 5×10^6 or 5×10^3 cells were inoculated under the back skin of B6 mice. Data are represented as mean values with S.D. ($n = 6$). (B) Doubling times of the cybrids under normal culture condition. Each experiment was performed in triplicate. (C) Cell invasion assay of the cybrids. Total numbers of 2.5×10^4 cells were seeded on the membrane, and the number of cells invaded through Matrigel basement membrane extract was counted using a modified Boyden chamber. Each experiment was performed in triplicate. (D) Migration assay of the cybrids. Total numbers of 1.25×10^4 cells were seeded on the membrane, and the number of migrated cells on the lower surface of the membrane was counted under a light microscope. Each experiment was performed in triplicate.

Then, we carried out sequence analysis for determination of mutations in C3H mtDNA responsible for the delayed tumor formation. Registered mtDNA sequences of B6 and C3H strains (Bayona-Bafaluy et al., 2003) revealed that four mutations, which are supposed to be polymorphic, are present in C3H mtDNA (Table 1). Of the four mutations, one is a missense mutation in the *COX3* (cytochrome *c* oxidase subunit 3) gene, one is a silent mutation in the *ND3* (NADH dehydrogenase subunit 3) gene, and the remaining two are insertion mutations in poly-T and poly-A tracts of the $tRNA^{Arg}$ gene. However, sequences of B6 mtDNA and C3H mtDNA in our cybrids may be different from the registered reference sequences (Kasahara et al., 2006). Therefore, we determined the whole mtDNA sequences of the cybrids, and found that mtDNA sequences of P29mtB6 and P29mtC3H are slightly different from the registered mtDNA sequences of B6 and C3H strains (Table 1): in addition to a missense mutation in the *COX3* gene, two missense mutations were present in the *ND2* (NADH dehydrogenase subunit 2) and in the *ND5* (NADH dehydrogenase subunit 5) genes, whereas no mutations were detectable in the $tRNA^{Arg}$ gene (Table 1). Thus, the three missense mutations in the *COX3*, *ND2*, and *ND5* genes can be responsible for the delay of tumor formation of P29mtC3H cybrids.

3.2. Effects of the absence of the immune systems in the B6 mice on the latent periods

First, we examined the possibility that immune systems in B6 mice are responsible for the delay of tumor formation. Our previous study (Ishikawa et al., 2010) showed that the innate immune system in B6 strain mice could recognize and suppress tumor formation of P29mtNZB cybrids with NZB mtDNA. Thus, the delay of tumor formation of P29mtC3H cybrids with C3H mtDNA in B6 mice also can be caused by innate and/or acquired immune systems of B6 mice. To test this idea, P29mtC3H cybrids were inoculated into the B6 $Rag2^{-/-}/\gamma c^{-/-}$ mice, which are deficient in both acquired and innate immune systems due to deficiency of recombination-activating gene ($Rag2^{-/-}$) and the common cytokine receptor gamma chain ($\gamma c^{-/-}$), and have no T cells, B cells, natural killer cells, and functional dendritic cells. However, the latent periods of P29mtC3H cybrids did not change substantially even in the immunodeficient B6 $Rag2^{-/-}/\gamma c^{-/-}$ mice (Fig. 2A).

To confirm this idea, P29mtC3H cybrids were inoculated into B6mtC3H congenic mice, which possess B6 nuclear genetic background but possess mtDNA from allogenic C3H mice. The results showed that the latent periods of tumor formation of P29mtC3H cybrids did not change substantially, even when the cybrids were injected into B6mtC3H mice, which share the same nuclear and mitochondrial genomes as those of the cybrids (Fig. 2B). These observations, together with the results shown in Fig. 2A, suggested that the delay of tumor formation of P29mtC3H cybrids in B6 mice would not be caused by immunological recognition of polymorphic mutations in C3H mtDNA, but probably by some abnormalities of mitochondrial respiratory function.

3.3. Comparison of respiration-related phenotypes between P29mtB6 and P29mtC3H cybrids

Even if the mutations in C3H mtDNA do not induce detectable respiration defects by biochemical analysis (Ishikawa et al., 2010), some abnormalities related to respiratory functions may be detectable. Therefore, we used P29mtB6 and P29mtC3H cybrids, and compared respiration-related phenotypes, such as cytochrome *c* oxidase (COX) activity, ROS and lactate production, and hypoxia sensitivity.

Table 1
Identification of candidate polymorphic mutations in mtDNA inducing a delay of tumor formation in P29mtC3H cybrids.

Position	C4794T	G9348A	T9461C	9818insT	9821insA	T12048C	15588	Accession no. [a]
Gene	*ND2*	*COX3*	*ND3*	$tRNA^{Arg}$	$tRNA^{Arg}$	*ND5*	D-loop	
Amino acid change	T294I	V248I	Silent	–	–	F103L	–	
C57BL/6J	C	G	T	3T	8A	T	C	AY172335
C3H/He	C	A	C	4T	9A	T	C	AB049357
P29mtB6	C	G	C	3T	9A	T	T	AP013030
P29mtC3H	T	A	C	3T	9A	C	C	AP013031

[a] Nucleotide sequence data reported are available in DDBJ/EMBL/GenBank databases under the Database ID: AY172335 (C57BL/6J), AB049357 (C3H/He), AP013030 (P29mtB6) and AP013031 (P29mtC3H).

Of the three missense mutations (C4794T in the *ND2*, G9348A in the *COX3*, and T12048C in the *ND5* genes), one G9348A mutation in the *COX3* gene can be a candidate mutation responsible for the delay of tumor formation of P29mtC3H cybrids, since G9348A mutation occurred in a site highly conserved throughout animals (Table 2). However, cytochemical analysis showed that COX activity was not reduced in P29mtC3H cybrids (Fig. 3A). In contrast, overproduction of mitochondrial ROS (superoxide) was observed in P29mtC3H cybrids (Fig. 3B). Moreover, overproduction of ROS (H_2O_2) from mitochondria was confirmed by using mitochondrial fraction from P29mtC3H cybrids (Fig. S1), and thus can be involved in delayed tumor formation in B6 mice (Fig. 1A).

In addition, we examined the possibility that decreased glycolysis of P29mtC3H cybrids resulted in the delayed tumor formation, since it has been proposed that the Warburg effect (increased glycolysis under normoxia) confers advantage of tumor growth under low O_2 condition (hypoxia). In fact, cybrids must survive and start growing under hypoxia on their inoculation under the back skin of B6 mice. Considering that the amounts of lactates reflect glycolytic activity, we estimated them, and found that lactates were not reduced in P29mtC3H cybrids (Fig. 3C), suggesting that the Warburg effects were not involved in this phenotype.

Another possibility to explain the delayed tumor formation of P29mtC3H cybrids is that they are sensitive to hypoxia, and require long latent periods to start growing under hypoxia. To examine this possibility we compared the hypoxia survival between P29mtB6 and P29mtC3H cybrids in hypoxic condition (<0.1% O_2). The results showed that P29mtC3H cybrids are more sensitive to hypoxia than P29mtB6 cybrids (Fig. 3D). These observations suggest that either ROS overproduction (Figs. 3B and S1) or hypoxia sensitive phenotype (Fig. 3D) exclusively observed in P29mtC3H cybrids would be responsible, at least in part, for the delay of tumor formation (Fig. 1A).

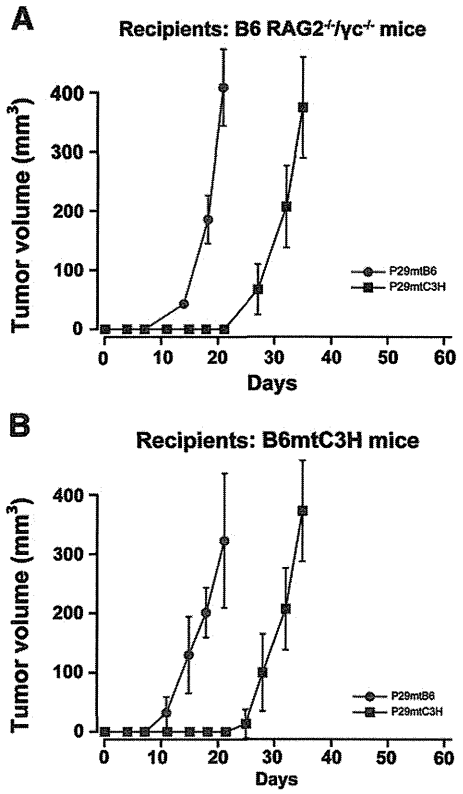

Fig. 2. Effects of absence of the immunological recognitions in the host B6 mice on the latent periods of tumor formation. Total numbers of 5×10^6 cells were inoculated under the skin of (A) B6 $Rag2^{-/-}/\gamma c^{-/-}$ mice, and (B) B6mtC3H mice to study the involvement of the immune systems in the tumor formation phenotypes of the cybrids ($n = 6$). The B6 $Rag2^{-/-}/\gamma c^{-/-}$ mice are severe combined immunodeficiency models that have macrophages and granulocytes, but no T cells, B cells, natural killer (NK) cells, or functional dendritic cells (DCs). The B6mtC3H mice are immunologically identical to P29mtC3H cybrids in their sharing the same nuclear and mitochondrial genetic backgrounds.

3.4. Effects of the pretreatment of the cybrids with NAC or hypoxia on latent periods

To examine the idea that ROS overproduction may result in the delay of tumor formation of P29mtC3H cybrids (Fig. 1A), they were pretreated with N-acetyl cysteine (NAC), one of the antioxidants, to exclude ROS, and then inoculated into B6 mice. As expected, NAC pretreatment reduced the amounts of ROS (Fig. 3B), but did not affect on the latency periods of tumor formation (Fig. 4A). Thus, ROS overproduction would not be involved in expression of the phenotype (Fig. 1A).

Then, we examined another possibility that P29mtC3H cybrids are sensitive to hypoxia (Fig. 3D), and thus require longer times than P29mtB6 cybrids for hypoxia adaptation. Hypoxic condition (<0.1% O_2) used to examine hypoxia survival (Fig. 3D) is not appropriate for hypoxia adaptation and subsequent inoculation of the cybrids, because the cybrids eventually die in <0.1% O_2. Therefore, 7% hypoxia was used for hypoxia adaptation to obtain sufficient number of the adapted cybrids for inoculation. For this, we pretreated the cybrids under 7% hypoxia for 21 days, which corresponded to the latent periods for

Table 2
Evolutionary conservation of the polymorphic mutations found in mtDNA from P29mtC3H cybrids.

Species	Accesion No.	Genes			
		ND2	*COX3*	*ND5*	D-loop
C57BL/6J	AY172335	FFYTRLI	VDVVWLF	IMQFSSW	ttaaac--taa
C3H/He	AB049357	FFYTRLI	VDVIWLF	IMQFSSW	ttaaac--taa
P29mtB6	AP013030	FFYTRLI	VDVVWLF	IMQFSSW	ttaaat--taa
P29mtC3H	AP013031	FFYIRLI	VDVIWLF	IMQLSSW	ttaaac--taa
Homo sapiens	NC_012920	YFYLRLI	VDVVWLF	IMEFSLW	cccaccctaa
Xenopus laevis	NC_001573	FFYLRLT	VDVVWLF	ILEFATW	tgtaactttaa
Danio rerio	AC024175	FFYLRLC	VDVVWLF	ILEFASW	tgtattatca-
Ciona savignyi	AB079784	VFYSRTM	VDVVWIF	ILNFAQW	-
Drosophila melanogaster	U37541	FFYLRIC	VDVVWLF	VIFYSKE	-
Caenorhabditis elegans	X54252	AFSFWLI	VDVVWLF	VLVFSTY	-
Saccharomyces cerevisiae	AJ011856	-	LDVIWLF	-	-
		291	*297*	*245*	*251*	*100*	*106*	

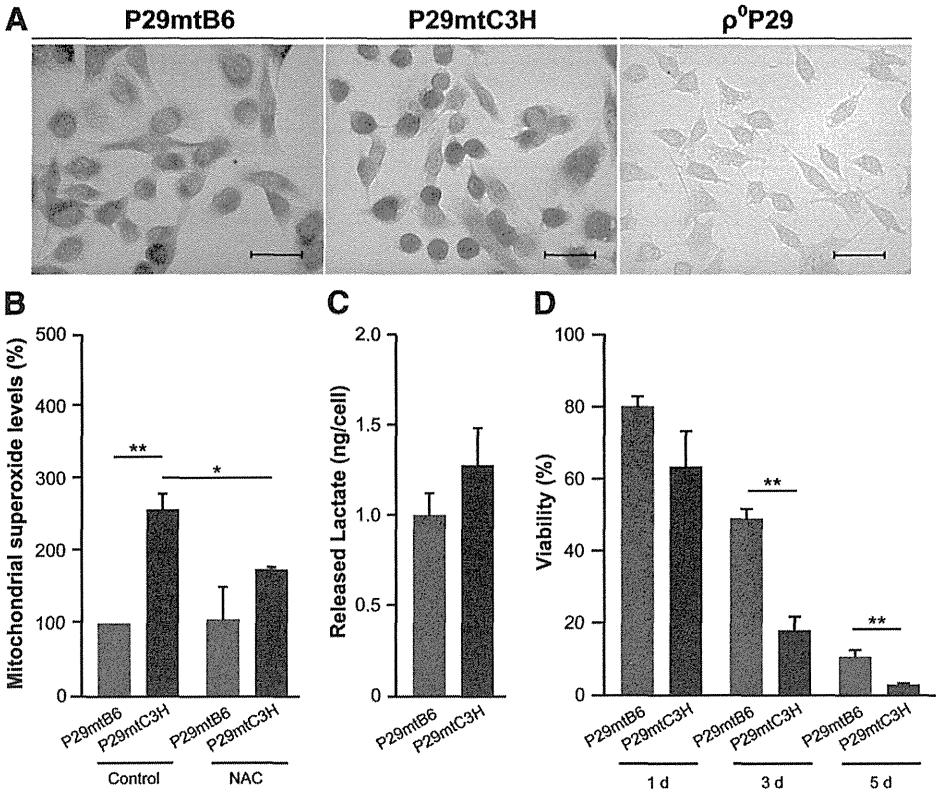

Fig. 3. Comparison of respiration-related phenotypes between P29mtB6 and P29mtC3H cybrids. (A) Cytochemical analysis of COX activity. ρ^0 P29 cells represent mtDNA-less (ρ^0) P29 cells, in which COX staining was not observed due to the absence of mtDNA and the resultant loss of COX activity. Scale bars, 100 mm. (B) Estimation of ROS (Mitochondrial superoxide) levels in the cybrids before and after their pretreatment with an antioxidant N-acetylcysteine (NAC) for 48 h. We used 20 mM NAC treatment, since our previous study (Ishikawa et al., 2008) showed that the concentration was sufficient to scavenge ROS and suppress ROS-induced metastasis. Relative ROS levels were expressed as mean fluorescence intensity. Data are represented as mean values with S.D. ($n = 3$). $^*P < 0.05$, $^{**}P < 0.01$. (C) Estimation of lactate levels in culture medium. Data are represented as mean values with S.D. ($n = 3$). (D) Viability of the cybrids under hypoxia. Sensitivity to hypoxia was determined by cultivation of the cells at 37 °C for 5 days under hypoxic conditions (<0.1% O_2). Data are represented as mean values with S.D. ($n = 3$). $^*P < 0.05$, $^{**}P < 0.01$.

tumor formation of P29mtC3H cybrids (Fig. 1A), and then inoculated them under the back skin of B6 mice to test the effect of hypoxia pretreatment on the latent periods. By pretreatment of P29mtC3H cybrids under hypoxia for 21 days, their latent periods were changed about 10 days shorter than those of untreated cybrids, while those of P29mtB6 cybrids did not change substantially (Fig. 4B). These observations suggest that some polymorphic mutations in C3H mtDNA induce a hypoxia sensitive phenotype, resulting in expression of long latent periods to adapt to hypoxic conditions under the skin of B6 mice.

To examine molecular mechanisms that explain the hypoxia sensitive phenotype of P29mtC3H cybrids, we compared the expression of the genes related to hypoxia, apoptosis, and autophagy between P29mtB6 and P29mtC3H cybrids. The results showed that enhanced expression of HIF-1α and phosphorylated AMPK (p-AMPK) was observed in P29mtC3H cybrids (Fig. 5). However, hypoxia adaptation did not suppress enhanced expression of HIF-1α and p-AMPK (Fig. 5), indicating that it would not directly regulate the delay of tumor formation of P29mtC3H cybrids (Fig. 1A).

4. Discussion

Our previous study (Ishikawa et al., 2010) revealed that polymorphic mutations in mtDNA from allogenic NZB strain mice were recognized by innate immune system in B6 mice, resulting in complete suppression of tumor formation of P29mtNZB cybrids. In contrast, P29mtC3H cybrids with allogenic C3H mtDNA were able to form tumors in B6 mice, although they showed longer latency periods to form detectable tumor masses than those of P29mtB6 cybrids with mtDNA from syngenic B6 strain mice. Because the retarded tumor formation found in P29mtC3H cybrids is also important as one of the tumor-related phenotypes, this study focused on the mechanisms of the retarded tumor formation observed in P29mtC3H cybrids.

We identified three missense mutations in C3H mtDNA by comparison of the whole mtDNA sequences between P29mtB6 and P29mtC3H cybrids, and addressed to the issue of how these mutations induce the retardation of tumor formation of P29mtC3H cybrids in B6 mice. The results suggested that the retardation was not due to the immunological recognition of P29mtC3H cybrids by host B6 immune systems or to ROS overproduction, but to the induction of the sensitivity to hypoxia. Probably, missense mutations in C3H mtDNA (Table 1) induce slight respiration defects that are not sufficient to be detected by our procedures, resulting in expression of hypoxia sensitivity and of long periods for P29mtC3H cybrids to adapt to the hypoxic conditions under the skin of B6 mice. However, the mechanisms of how the C3H mtDNA mutations induce hypoxia sensitivity and delayed tumor formation are complicated, and we could not at present explain the precise mechanisms.

It has been proposed that polymorphic mutations in poly-A tracts (10A repeats) of the *tRNA^{Arg}* gene found in the cybrids with mtDNA from NZB strain mice and from NIH3T3 cells induced overproduction of ROS (Moreno-Loshuetros et al., 2006). Although P29mtC3H cybrids with mtDNA from C3H strain also overproduced ROS, our mtDNA sequence data (Table 1) showed that both mtDNAs from P29mtB6 and P29mtC3H cybrids shared the same poly-A tracts (9A repeats) in the *tRNA^{Arg}* gene. Moreover, pretreatment of P29mtC3H cybrids with an antioxidant (NAC) did not affect the prolonged latent periods for tumor formation (Fig. 4A). Thus, ROS overproduction in P29mtC3H cybrids would not be caused by mutations in the *tRNA^{Arg}* gene, and would not be responsible for the delay of tumor formation.

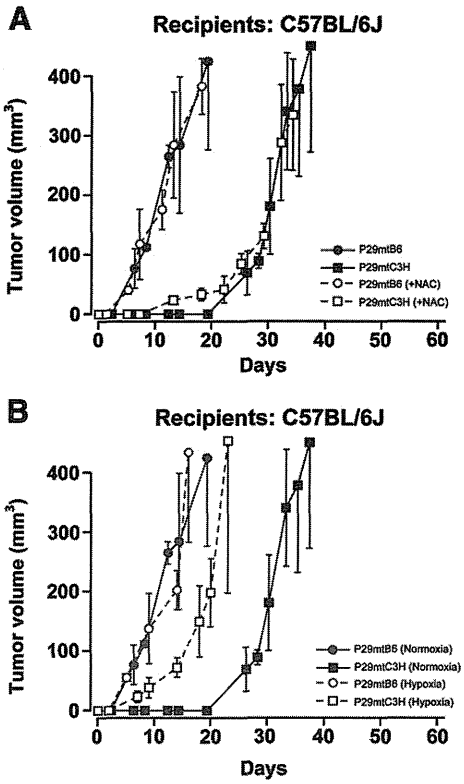

Fig. 4. Effects of the pretreatment of the cybrids with NAC or hypoxia on their latent periods for tumor formation. (A) NAC pretreatment. The cybrids were inoculated under the skin of B6 mice after their pretreatment with 20 mM NAC for 48 h, and host B6 mice were furthermore given 60 mM NAC in drinking water *ad libitum*. (B) Hypoxia pretreatment. The cybrids were inoculated under the skin of B6 mice after their pretreatment with hypoxia for 21 days. The retardation of tumor formation exclusively observed in P29mtC3H cybrids (Fig. 1A) was improved by their pretreatment with hypoxia but not with NAC.

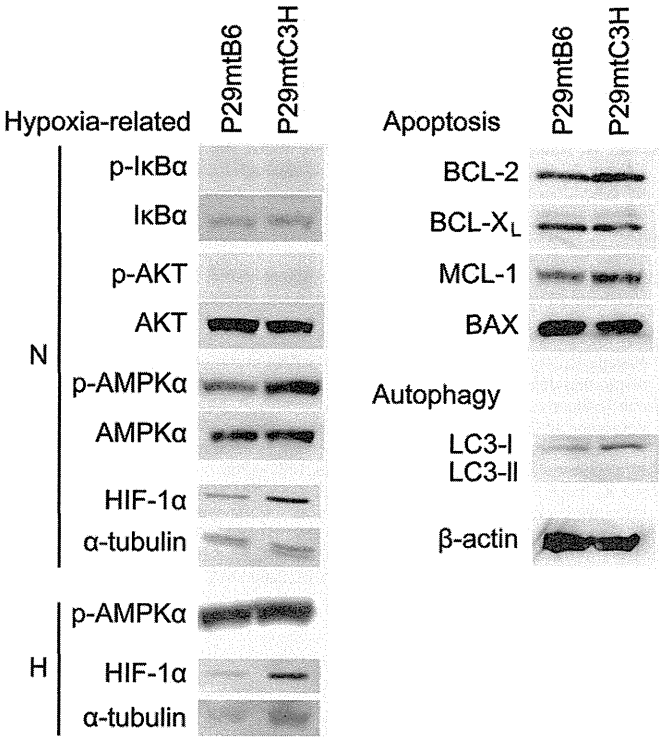

Fig. 5. Examination of the genes related to the retardation of the tumor formation observed in P29mtC3H cybrids. Western blot analysis was carried out about the genes associated with hypoxia, apoptosis, and autophagy. The gene products associated with hypoxia were examined under normoxia (N), and then those of HIF-1α and p-AMPK overexpressed in P29mtC3H cybrids were also examined after hypoxia adaptation under 7% O_2 for 21 days (H).

This study revealed that polymorphic mutations in mtDNA affect a tumor-related phenotype. Involvement of polymorphic mtDNA mutations in expression of tumor phenotypes was proposed based on the evidence that most mtDNA mutations found in tumors were polymorphic mutations (Loeb et al., 2005; Wallace, 2005). Moreover, polymorphic mtDNA mutations were proposed to affect age-related hearing loss (Johnson et al., 2001), learning retardation (Roubertoux et al., 2003), and delay of cell proliferation (Moreno-Loshuertos et al., 2006). Furthermore, our previous study (Ishikawa et al., 2010) revealed a novel role of polymorphic mutations in mouse mtDNA by showing that the innate immune system in B6 strain mice can recognize and suppress tumor formation of P29mtNZB cybrids with mtDNA introduced from allogenic NZB strain mice.

Therefore, we have to be careful for polymorphic mutations as well as pathogenic mutations in human mtDNA, particularly when we carry out transplantation of tissues differentiated from iPS cells, and nuclear transplantation to human oocytes for the gene therapy of mitochondrial diseases. For example, the mtDNA in iPS cells might accumulate such somatic mutations that can be recognized by innate immune systems or induce hypoxia sensitivity during the aging of the donors, resulting in expression of some unexpected disorders in transplanted tissues. Moreover, one of the most important problems that have to be resolved before applying the nuclear transplantation technology (Craven et al., 2010; Tachibana et al., 2013) to the human oocytes from mothers with mitochondrial diseases is the influence of polymorphic mutations in mtDNA of the oocyte donors on the phenotypes of the progeny, even when the polymorphic mutations do not induce significant respiration defects.

Supplementary data to this article can be found online at http://dx.doi.org/10.1016/j.mito.2013.07.117.

Acknowledgments

This work was supported by Grants-in-Aid for Scientific Research A 25250011 (to J.-I.H.), Scientific Research A 23240058 (to K.N.), and Scientific Research on Innovative Areas 24117503 (to J.-I.H.) from Japan Society for the Promotion of Science. This work was also supported by Grant-in-Aid for JSPS Fellows (to H. I.), and by World Premier International Research Center Initiative (WPI), MEXT, Japan (to K.N. and J.-I.H.).

References

Bayona-Bafaluy, M.P., Acín-Pérez, R., Mullikin, J.C., Park, J.S., Moreno-Loshuertos, R., Hu, P., Pérez-Martos, A., Fernández-Silva, P., Bai, Y., Enríquez, J.A., 2003. Revisiting the mouse mitochondrial DNA sequence. Nucleic Acids Res. 31, 5349–5355.

Craven, L., Tuppen, H.A., Greggains, G.D., Harbottle, S.J., Murphy, J.L., Cree, L.M., Murdoch, A.P., Chinnery, P.F., Taylor, R.W., Lightowlers, R.N., Herbert, M., Turnbull, D.M., 2010. Pronuclear transfer in human embryos to prevent transmission of mitochondrial DNA disease. Nature 465, 82–85.

Hashizume, O., Shimizu, A., Yokota, M., Sugiyama, A., Nakada, K., Miyoshi, H., Itami, M., Ohira, M., Nagase, H., Takenaga, K., Hayashi, J.-I., 2012. Specific mitochondrial DNA mutation in mice regulates diabetes and lymphoma development. Proc. Natl. Acad. Sci. U.S.A. 109, 10528–10533.

Imanishi, H., Hattori, K., Wada, R., Ishikawa, K., Fukuda, S., Takenaga, K., Nakada, K., Hayashi, J.-I., 2011. Mitochondrial DNA mutations regulate metastasis of human breast cancer cells. PLoS One 6, e23401.

Inoue, K., Nakada, K., Ogura, A., Isobe, K., Goto, Y., Nonaka, I., Hayashi, J.-I., 2000. Generation of mice with mitochondrial dysfunction by introducing mouse mtDNA carrying a deletion into zygotes. Nat. Genet. 26, 176–181.

Ishikawa, K., Takenaga, K., Akimoto, M., Koshikawa, N., Yamaguchi, A., Imanishi, H., Nakada, K., Honma, Y., Hayashi, J.-I., 2008. ROS-generating mitochondrial DNA mutations can regulate tumor cell metastasis. Science 320, 661–664.

Ishikawa, K., Toyama-Sorimachi, N., Nakada, K., Morimoto, M., Imanishi, H., Yoshizaki, M., Sasawatari, S., Niikura, M., Takenaga, K., Yonekawa, H., Hayashi, J.-I., 2010. The innate

immune system in host mice targets cells with allogenic mitochondrial DNA. J. Exp. Med. 207, 2297–2305.
Jacobs, H.T., 2003. The mitochondrial theory of aging: dead or alive? Aging Cell 2, 11–17.
Johnson, K.R., Zheng, Q.Y., Bykhovskaya, Y., Spirina, O., Fischel-Ghodsian, N., 2001. A nuclear– mitochondrial DNA interaction affecting hearing impairment in mice. Nat. Genet. 27, 191–194.
Kasahara, A., Ishikawa, K., Yamaoka, M., Ito, M., Watanabe, N., Akimoto, M., Sato, A., Nakada, K., Endo, H., Suda, Y., Aizawa, S., Hayashi, J.-I., 2006. Generation of trans-mitochondrial mice carrying homoplasmic mtDNA with a missense mutation in a structural gene using ES cells. Hum. Mol. Genet. 15, 871–881.
Khrapko, K., Vija, J., 2008. Mitochondrial DNA mutations and aging: devils in the details? Trends Genet. 25, 91–98.
Loeb, L.A., Wallace, D.C., Martin, G.M., 2005. The mitochondrial theory of aging and its relationship to reactive oxygen species damage and somatic mtDNA mutations. Proc. Natl. Acad. Sci. U.S.A. 102, 18769–18770.
Mito, T., Kikkawa, Y., Shimizu, A., Hashizume, O., Katada, S., Imanishi, H., Ota, A., Kato, Y., Nakada, K., Hayashi, J.-I., 2013. Mitochondrial DNA mutations in mutator mice confer respiration defects and B-cell lymphoma development. PLoS One 8, e55789.
Moreno-Loshuertos, R., Acín-Pérez, R., Fernández-Silva, P., Movilla, N., Pérez-Martos, A., Rodriguez de Cordoba, S., Gallardo, M.E., Enríquez, J.A., 2006. Differences in reactive oxygen species production explain the phenotypes associated with common mouse mitochondrial DNA variants. Nat. Genet. 38, 1261–1268.
Nakada, K., Inoue, K., Ono, T., Isobe, K., Ogura, A., Goto, Y.I., Nonaka, I., Hayashi, J.-I., 2001. Inter-mitochondrial complementation: mitochondria-specific system preventing mice from expression of disease phenotypes by mutant mtDNA. Nat. Med. 7, 934–940.
Paull, D., Emmanuele, V., Weiss, K.A., Treff, N., Stewart, L., Hua, H., Zimmer, M., Kahler, D.J., Goland, R.S., Noggle, S.A., Prosser, R., Hirano, M., Sauer, M.V., Egli, D., 2013. Nuclear genome transfer in human oocytes eliminates mitochondrial DNA variants. Nature 493, 632–637.
Roubertoux, P.L., Sluyter, F., Carlier, M., Marcet, B., Maarouf-Veray, F., Chérif, C., Marican, C., Arrechi, P., Godin, F., Jamon, M., Verrier, B., Cohen-Salmon, C., 2003. Mitochondrial DNA modifies cognition in interaction with the nuclear genome and age in mice. Nat. Genet. 35, 65–69.
Sato, A., Kono, T., Nakada, K., Ishikawa, K., Inoue, S., Yonekawa, H., Hayashi, J.-I., 2005. Gene therapy for progeny of mito-mice carrying pathogenic mtDNA by nuclear transplantation. Proc. Natl. Acad. Sci. U.S.A. 102, 16765–16770.
Seligman, A.M., Karnovsky, M.J., Wasserkrug, H.L., Hanker, J.S., 1968. Nondroplet ultrastructural demonstration of cytochrome oxidase activity with a polymerizing osmiophilic reagent, diaminobenzidine (DAB). J. Cell Biol. 38, 1–14.
Sharpley, M.S., Marciniak, C., Eckel-Mahan, K., McManus, M., Crimi, M., Waymire, K., Lin, C.S., Masubuchi, S., Friend, N., Koike, M., Chalkia, D., MacGregor, G., Sassone-Corsi, P., Wallace, D.C., 2012. Heteroplasmy of mouse mtDNA is genetically unstable and results in altered behavior and cognition. Cell 151, 333–343.
Tachibana, M., Sparman, M., Sritanaudomchai, H., Ma, H., Clepper, L., Woodward, J., Li, Y., Ramsey, C., Kolotushkina, O., Mitalipov, S., 2009. Mitochondrial gene replacement in primate offspring and embryonic stem cells. Nature 461, 367–372.
Tachibana, M., Amato, P., Sparman, M., Woodward, J., Sanchis, D.M., Ma, H., Gutierrez, N.M., Tippner-Hedges, R., Kang, E., Lee, H.S., Ramsey, C., Masterson, K., Battaglia, D., Lee, D., Wu, D., Jensen, J., Patton, P., Gokhale, S., Stouffer, R., Mitalipov, S., 2013. Towards germline gene therapy of inherited mitochondrial diseases. Nature 493, 627–631.
Taylor, R.W., Turnbull, D.M., 2005. Mitochondrial DNA mutations in human disease. Nat. Rev. Genet. 6, 389–402.
Wallace, D.C., 2005. A mitochondrial paradigm of metabolic and degenerative diseases, aging, and cancer: a dawn for evolutionary medicine. Annu. Rev. Genet. 39, 359–407.

Mitochondrial DNA with a Large-Scale Deletion Causes Two Distinct Mitochondrial Disease Phenotypes in Mice

Shun Katada,* Takayuki Mito,* Emi Ogasawara,† Jun-Ichi Hayashi,†,‡ and Kazuto Nakada†,1
*Graduate School of Life and Environmental Sciences, †Faculty of Life and Environmental Sciences, and ‡International Institute for Integrative Sleep Medicine (WPI-IIIS), University of Tsukuba, 1-1-1 Tennoudai, Tsukuba, Ibaraki 305-8575, Japan

ABSTRACT Studies in patients have suggested that the clinical phenotypes of some mitochondrial diseases might transit from one disease to another (e.g., Pearson syndrome [PS] to Kearns-Sayre syndrome) in single individuals carrying mitochondrial (mt) DNA with a common deletion (ΔmtDNA), but there is no direct experimental evidence for this. To determine whether ΔmtDNA has the pathologic potential to induce multiple mitochondrial disease phenotypes, we used *trans*-mitochondrial mice with a heteroplasmic state of wild-type mtDNA and ΔmtDNA (mito-miceΔ). Late-stage embryos carrying ≥50% ΔmtDNA showed abnormal hematopoiesis and iron metabolism in livers that were partly similar to PS (PS-like phenotypes), although they did not express sideroblastic anemia that is a typical symptom of PS. More than half of the neonates with PS-like phenotypes died by 1 month after birth, whereas the rest showed a decrease of ΔmtDNA load in the affected tissues, peripheral blood and liver, and they recovered from PS-like phenotypes. The proportion of ΔmtDNA in various tissues of the surviving mito-miceΔ increased with time, and Kearns-Sayre syndrome–like phenotypes were expressed when the proportion of ΔmtDNA in various tissues reached >70–80%. Our model mouse study clearly showed that a single ΔmtDNA was responsible for at least two distinct disease phenotypes at different ages and suggested that the level and dynamics of ΔmtDNA load in affected tissues would be important for the onset and transition of mitochondrial disease phenotypes in mice.

KEYWORDS
mitochondria
mitochondrial DNA
pathogenic mutation
mitochondrial diseases
model mice

Pathogenic mtDNAs having a large-scale deletion (ΔmtDNA), called the "common deletion," or a point mutation, induce defects of mitochondrial oxidative phosphorylation (mitochondrial respiration defects) and manifest as a wide variety of mitochondrial diseases (Larsson and Clayton 1995; Wallace 1999). It has been well documented that ΔmtDNA is responsible for three clinical phenotypes of mitochondrial diseases: Kearns–Sayre syndrome (KSS), progressive external ophthalmoplegia, and Pearson syndrome (PS) (DiMauro and Garone 2011). KSS is usually sporadic and is characterized by early onset (<20 years of age), lactic acidosis, chronic progressive external ophthalmoplegia, pigmentary retinopathy, heart block, diabetes, deafness, cerebellar abnormalities, and renal failure. Progressive external ophthalmoplegia is mainly a skeletal muscle disorder and is characterized by late-onset progressive external ophthalmoplegia, lactic acidosis, myopathy, and exercise intolerance. PS is a rare disorder of early infancy that is characterized mainly by sideroblastic anemia. At present, the precise mechanism by which ΔmtDNA can cause different disease phenotypes is unclear, although it has been considered that different loads of ΔmtDNA in tissues are important to establish the multiple disease phenotypes.

Some studies in patients have reported the possibility that infants with PS who survive into childhood develop the clinical features of KSS (Larsson *et al.* 1990; McShane *et al.* 1991; Rotig *et al.* 1995). Furthermore, Larsson *et al.* (1990) suggest that the transition of disease phenotypes is governed by the fractional concentration of ΔmtDNA in various tissues; however, there is currently no experimental

doi: 10.1534/g3.113.007245
Manuscript received May 20, 2013; accepted for publication July 2, 2013

[1]Corresponding author: Faculty of Life and Environmental Sciences, University of Tsukuba, 1-1-1 Tennoudai, Tsukuba, Ibaraki 305-8572, Japan. E-mail: knakada@biol.tsukuba.ac.jp

evidence for this. Because mitochondrial function is regulated both by nuclear DNA and mtDNA (Larsson and Clayton 1995), it is possible that nuclear genomic background is involved in the pathogenesis of different disease phenotypes. Supporting this hypothesis is the finding that the homoplasmic state of a pathogenic mutant mtDNA does not always induce serious clinical phenotypes in a mother and her children (McFarland *et al.* 2002).

Here, to experimentally resolve the question of whether mitochondrial disease phenotypes can change in single individuals as a result of the dynamics of the proportion of ΔmtDNA in various tissues, we have used a mouse model carrying pathogenic ΔmtDNA. Previously, we succeeded in generating a *trans*-mitochondrial mouse model (mito-miceΔ) with a heteroplasmic state for wild-type mtDNA and ΔmtDNA with a 4696-bp deletion from nucleotide position 7759 of the $tRNA^{Lys}$ gene to position 12,454 of the *ND5* gene (see Figure 1A) (Inoue *et al.* 2000). The ΔmtDNA introduced in mito-miceΔ is similar to the pathogenic mutant mtDNA with the "common deletion" that is found in patients with KSS or PS (Holt *et al.* 1988; Larsson *et al.* 1990; McShane *et al.* 1991; Rotig *et al.* 1995). Because the mito-miceΔ all share the same nuclear genomic background (C57BL/6, also called B6), their genetic variation is restricted to the load of ΔmtDNA in various tissues. The mito-miceΔ, therefore, would provide the direct experiment evidence whether a single ΔmtDNA could cause the onset and transition of different mitochondrial disease phenotypes.

By using these mito-miceΔ, we investigated that ΔmtDNA possessed a pathogenic potential for the onset of two distinct phenotypes of mitochondrial diseases, PS-like and KSS-like phenotypes, early in life (days 1−34 after birth) and in midlife (6 months of age), respectively. We also observed that the mice that escaped from the early death probably because PS-like phenotypes developed KSS-like phenotypes in middle age, showing the transition of distinct mitochondrial disease phenotypes in single mito-miceΔ.

MATERIALS AND METHODS

Mice

Mito-miceΔ were generated by introducing ΔmtDNA from cultivated cells into the zygotes of B6 strain mice by using cell fusion techniques, as described previously (Inoue *et al.* 2000). Thirty-three female mito-miceΔ carrying 1–63% ΔmtDNA at 2–6 months of age were used as mothers. Embryos on E18.5 and progeny were used for the study. Age-matched wild-type B6 mice were used as normal controls. All animal experiments were performed in compliance with the institutional guidelines of the University of Tsukuba for the care and use of laboratory animals.

Estimation of ΔmtDNA proportion in tissues

Proportions of wild-type mtDNA and ΔmtDNA were determined by using real-time polymerase chain reaction, as described previously (Sato *et al.* 2005). Tail samples were used to deduce the ΔmtDNA load in mito-miceΔ. The proportion of ΔmtDNA was also examined in various tissue samples (peripheral blood, liver, kidney, and eye).

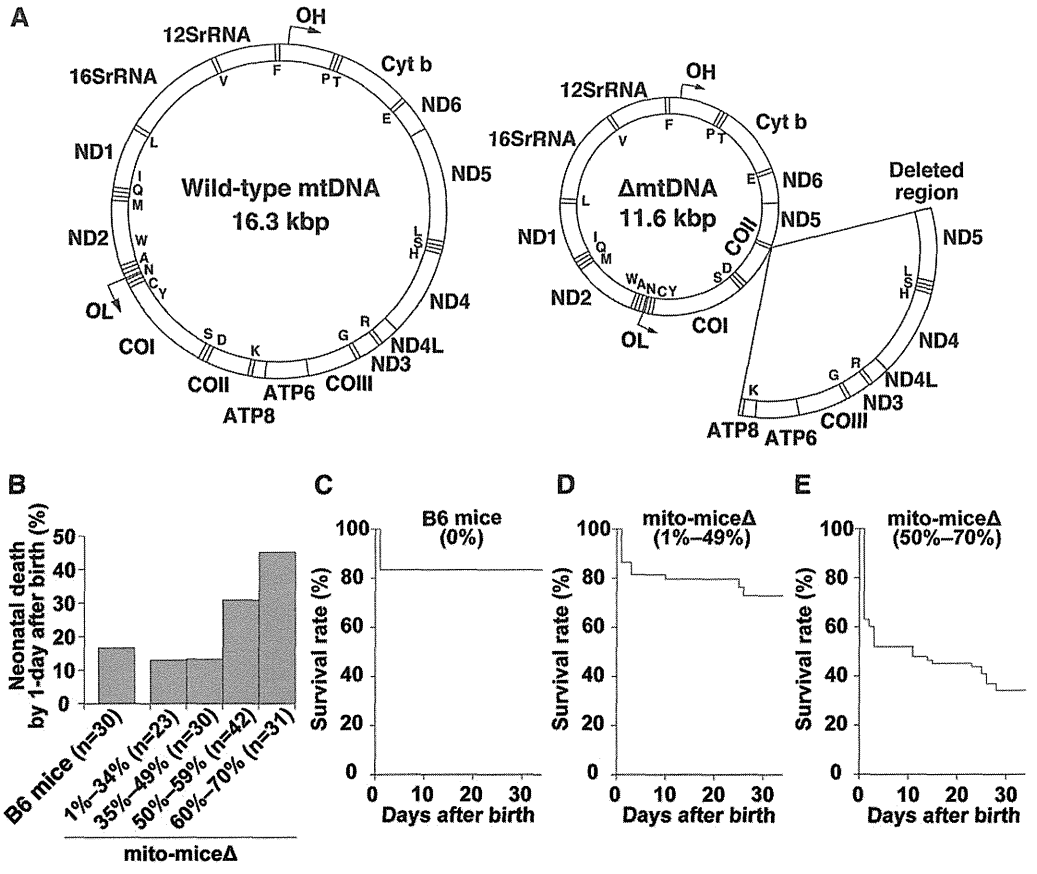

Figure 1 Gene map of ΔmtDNA introduced in mito-miceΔ and observations of mito-miceΔ on the early life. (**A**) A wild-type mtDNA (left) is a circular DNA (16.3 kbp) and encodes 37 genes, including 13 mRNAs, 22 tRNAs, and 2 rRNAs. A mtDNA with a common deletion (ΔmtDNA; right) introduced in mito-miceΔ is 11.3 kbp in size, because 13 genes, including 7 mRNAs and 6 tRNAs (arc) are lost by a deletion. Single capitals in maps indicate tRNA genes. (B) Frequency of neonatal death in mito-miceΔ carrying 1–70% ΔmtDNA in their tails. Neonates of mito-miceΔ were classified into four groups carrying 1–34% (n = 23), 35–49% (n = 30), 50–59% (n = 42), and 60–70% (n = 31) ΔmtDNA, respectively, in their tails. Neonates of wild-type B6 mice were used as normal controls (n = 30). (C–E) Life span of mito-miceΔ carrying 1–70% ΔmtDNA in their tails was assessed for days 1 to 34. Based on the observed frequency of neonatal death in mito-miceΔ (see panel B), neonates of mito-miceΔ were classified into two groups carrying 1–49% (n = 53) (D) and 50–70% (n = 73) (E) ΔmtDNA in their tails, and the life span of each group was examined. The life span of wild-type B6 mice was also examined as a normal control (n = 30) (C). Survival curves were compared between mito-miceΔ carrying 1–49% ΔmtDNA and wild-type B6 mice (P = 0.3054, log-rank test) and between mito-miceΔ carrying 50–70% ΔmtDNA and wild-type B6 mice ($P < 0.0001$, log-rank test).

Measurement of blood lactate concentration

For the measurement of blood lactate concentration, blood was collected from the tail vein of nonfasted mice. Lactate concentration was measured by using an automatic blood lactate test meter (Lactate Pro, ARKRAY, Kyoto, Japan).

Cytologic and histologic analysis

Blood samples were smeared on glass slides, and inclusions in reticulocytes were visualized by staining with new methylene blue. Cells with granular network inclusions that are a typical structure of reticulocytes were counted (see open arrowheads in Figure 3D) and proportion of these reticulocytes to 1000 red blood cells was estimated. The proportion of reticulocytes in blood samples of mito-miceΔ and age-matched controls was measured. To detect the accumulation of ferric iron, paraffin-embedded sections (5-μm thick) of liver samples were stained with Prussian blue and then Safranin O was used as a counter-staining. Eye samples were fixed in Bouin's solution, and paraffin-embedded sections (8-μm thick) of the samples were stained with hematoxylin and eosin.

Electron microscopic observation of cytochrome c oxidase (COX) activity

An electron microscopic analysis of COX activity was performed as described previously (Nakada *et al.* 2001; Seligman *et al.* 1968) with slight modifications. To summarize, 25-μm cryosections of liver samples were fixed in 2% w/v glutaraldehyde in phosphate-buffered saline for 5 min at 0°. Ultrathin sections, which were not stained with uranyl acetate or lead nitrate solutions, were viewed directly on a transmission electron microscope (model H-7650, Hitachi High-Technologies Corporation, Tokyo, Japan). In this analysis, enzymatic activity of COX was visualized as a black color (high electron density).

Statistics

The Student's *t*-test was used to compare groups of data. All values are presented as means ± SD. The log-rank test was used to compare survival curves. $P < 0.05$ was considered to indicate statistical significance.

RESULTS

Frequency of early death in mito-miceΔ

We first examined the early life spans (1–34 days after birth) of mito-miceΔ carrying 1–70% ΔmtDNA in their tails (n = 126). The proportion of ΔmtDNA in individual mito-miceΔ was deduced from that in their tails just after birth (day 0). In this assay, we also used wild-type B6 mice as a normal control (n = 30). Approximately 20% of wild-type B6 neonates died on day 1 after birth (Figure 1B), but none died from days 2 to 34 (Figure 1C). The early life spans of mito-miceΔ carrying <50% ΔmtDNA in their tails were similar to those of wild-type B6 mice (Figure 1, C and D). In contrast, when the ΔmtDNA load in the neonates' tails was ≥50%, the frequency of death on day 1 after birth was definitely increased compared with that of wild-type B6 mice (Figure 1B). The mito-miceΔ carrying 50–70% ΔmtDNA in their tails continued to die after day 1, and only 34% of these neonates survived until day 34 after birth (Figure 1E).

Although the aforementioned results indicated that most mito-miceΔ carrying ≥50% ΔmtDNA died early (≤34 days after birth), a substantial proportion of the progeny of mothers carrying >33% ΔmtDNA died very early (day 1 after birth; Figure 2A). Thus, it was unclear that early death was associated with the proportion of ΔmtDNA either in neonates or mothers. If the latter were the case, then the frequency of early death of pups would be expected to increase with the age of the mother, because ΔmtDNA accumulates in various somatic tissues but disappears in eggs with time (Sato *et al.* 2007). Therefore, we next examined the frequency of early death in the first and second litters of three female mito-miceΔ carrying 28% (Mouse 28), 52% (Mouse 52), and 61% (Mouse 61) ΔmtDNA, respectively, in their tails just after birth. As expected, the proportion of ΔmtDNA was much greater in the first litter than the second litter (Figure 2B). The rate of early death of pups was greatly and significantly greater in the first litter than in the second delivery (Figure 2, B and C; $P < 0.05$). The proportion of surviving pups from the second litter (Figure 2C) was comparable with that of pups with wild-type B6 mothers (Figure 1B), despite the ΔmtDNA load of the mothers' tails increasing with time. Average loads of ΔmtDNA in tail samples were 32.4 ± 21.9% (mean ± SD) and 57.4 ± 16.8% in live and dead mito-miceΔ pups, respectively. On the basis of these results, we concluded that early death of mito-miceΔ was caused by ΔmtDNA load in neonates but not in mothers.

Phenotypic observations of late-stage embryos of mito-miceΔ

To clarify the reason for the frequent early death in progeny carrying ≥50% ΔmtDNA in their tails, we examined clinical phenotypes in embryos at embryonic day 18.5 (E18.5), which is just 1 day before birth. We obtained 55 E18.5 embryos carrying 35–70% ΔmtDNA in

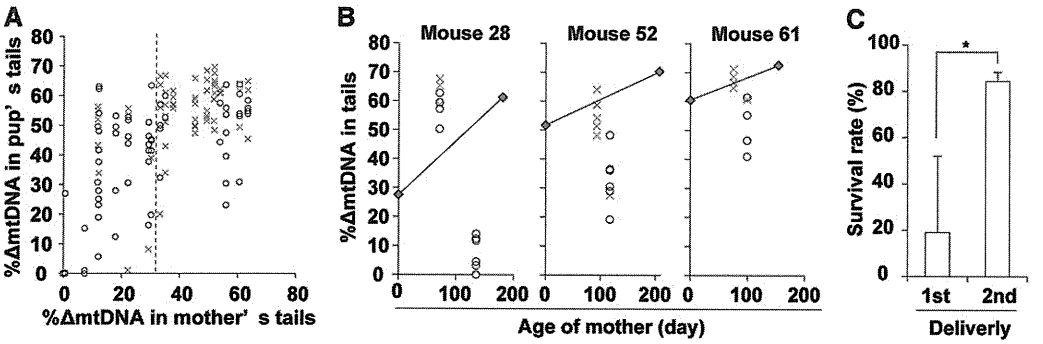

Figure 2 Relationship between early death and ΔmtDNA load in mito-miceΔ. (A) Comparison of ΔmtDNA proportion in tail samples from pups and mothers. Open circles and red crosses indicate pups that were alive and dead, respectively, at 34 days after birth. (B) Comparison between first and second litters in terms of pup survival and ΔmtDNA proportion in the tails of pups. Three female mito-miceΔ carrying 28% (Mouse 28), 52% (Mouse 52), and 61% (Mouse 61) ΔmtDNA in their tails just after birth (day 0) were used in this assay. Open circles and red crosses indicate the proportions of ΔmtDNA in the tails of pups that were alive and dead, respectively, at 34 days after birth. Blue symbols indicate the proportions of ΔmtDNA in mother's tails. (C) Comparison between the first and second deliveries in terms of survival rates of pups from Mouse 28, Mouse 52, and Mouse 61 at day 34 after birth. Data are presented as mean ± SD. Asterisk indicates significant differences ($P < 0.05$).